Universidade de Aveiro

Departamento de Química

2022

Raquel Dias Dantas

Novos eléctrodos à base de materiais porosos redox-ativos para baterias mais eficientes

New electrodes based on redox-active porous materials towards more efficient batteries

Universidade de Aveiro

Departamento de Química

2022

Raquel Dias Dantas

Novos eléctrodos à base de materiais porosos redox-ativos para baterias mais eficientes

New electrodes based on redox-active porous materials towards more efficient batteries

Dissertação apresentada à Universidade de Aveiro para cumprimento dos requisitos necessários à obtenção do grau de Mestre em Engenharia Química, realizada sob a orientação científica do Professor Doutor Manuel Souto Salom, Professor Auxiliar do Departamento de Química da Universidade de Aveiro e co-orientação do Professor Doutor João Rocha, Professor Catedrático do Departamento de Química da Universidade de Aveiro.

Trabalho financiado pela Bolsa de Investigação (BII) no âmbito do projeto/unidade de I&D "Redox-active Metal-Organic Frameworks as Electrode Materials for Lithium-Ion Batteries (RedoxMOFs)" (PTDC/QUI-ELT/2593/2021). Da Fundação para a Ciência e a Tecnologia, I.P./MCTES, através de fundos nacionais (PIDDAC).

o júri

presidente

Doutora Maria Inês Purcell de Portugal Branco
Professora Auxiliar do Departamento de Química da Universidade de Aveiro

Doutora Maria Helena Sousa Soares de Oliveira Braga
Professora Associada da Faculdade de Engenharia da Universidade do Porto

Doutor Manuel Souto Salom
Professor Auxiliar do Departamento de Química da Universidade de Aveiro

agradecimentos

O meu maior agradecimento não poderá deixar de ser dirigido ao meu orientador, o Professor Manuel Souto. Por toda a orientação, constante disponibilidade e incentivo. Por todas as oportunidades, por toda a ajuda e por todo o apoio e acompanhamento ao longo deste ano. Um enorme agradecimento também ao Professor João Rocha pela disponibilidade, apoio e incentivo. É sem dúvida contagiante a paixão que têm pela ciência.

Ao Gonçalo, por me ter acompanhado incansavelmente desde o meu primeiro dia no laboratório, por responder a todas as minhas perguntas, ainda que repetitivas e por ter sempre uma palavra de apoio quando eu mais preciso dela.

Aos meus colegas do laboratório, o Pedro e a Catarina, um agradecimento por toda a ajuda e colaboração e acima de tudo por fazerem do laboratório uma segunda casa. E ainda, à Isabel, por toda a ajuda no laboratório e pela constante disponibilidade.

Ao grupo MatER da FEUP que tão bem me recebeu e me fez sentir parte da família. Um agradecimento especial ao Nuno por toda a ajuda no laboratório. Por fim, um agradecimento gigante à professora Helena, por toda a ajuda, boa disposição e energia contagiante, por toda a paciência e acima de tudo por todo o conhecimento.

À Maria Oliveira, por estar sempre perto ainda que longe fisicamente. Um agradecimento especial pela ilustração da minha *coin-cell* mas acima de tudo obrigada por todo o teu apoio. À Bárbara e à Elisabete, que tantas vezes me puxaram para continuar quando queria desistir. Obrigada por todos os bons momentos e por estarem sempre presentes, quer há distância de um passo, quer de uns bons quilómetros.

Ao BEST Aveiro, que durante todo o meu percurso académico me proporcionou grandes oportunidades de crescimento e desenvolvimento pessoal, muitos bons momentos e acima de tudo colocou no meu caminho pessoas maravilhosas. Um agradecimento especial aos que se tornaram amigos próximos e uma fonte de contante apoio e inspiração.

Por fim, um agradecimento gigante do fundo do coração à minha família. Que sorte enorme poder ter-vos comigo, nos bons e maus momentos, perto ou longe.

À minha irmã, Bruna, pela preocupação, apoio e carinho. E mais que tudo, um agradecimento incondicional à minha mãe. Por todo o amor, por toda a dedicação, por toda a força, por todo o suor e lágrimas. Sem ti, sem o teu apoio e sem o teu esforço nada disto seria possível e nunca haverá palavras suficientes para te agradecer.

Por fim, à minha avó, que sempre me incentivou incansavelmente. Obrigada por todo o amor e por toda a força.

Obrigada!

palavras-chave

Estruturas Orgânicas Covalentes; Elétrodos orgânicos; Baterias de ião lítio, Armazenamento de energia.

resumo

Atualmente, o setor energético continua a ser o principal contribuidor para o aquecimento global, tornando cada vez mais urgente a transição energética de combustíveis fósseis para fontes de energia mais limpas. Devido ao problema da disponibilidade intermitente de energia de origem renovável, há uma necessidade cada vez maior para soluções de armazenamento energético melhores, mais seguras e mais sustentáveis. Esta dissertação foca-se no uso de Estruturas Orgânicas Covalentes (COFs), um tipo de polímero orgânico, para o uso como material ativo em elétrodos de baterias ião lítio. Numa fase inicial, o trabalho focou-se na síntese e caracterização de novos materiais porosos redox-ativos, assim como, no design de novos COFs com condutividade elétrica mais elevada. Posteriormente, os matérias sintetizados foram usados como elétrodos em baterias. Para esse fim, o processo de preparação do elétrodo foi otimizado e as baterias fabricadas e testadas. Assim, foram analisadas as relações entre as estruturas orgânicas covalentes e a sua aplicação em materiais de armazenamento energético.

keywords

Covalent organic frameworks; Organic electrodes; Lithium-ion batteries; Energy storage.

abstract

Today the energy sector is still the main contributor towards global warming, raising the urgency for a faster transition from fossil fuels to cleaner energy sources. Due to the renewable's intermittent availability problem, there is an increased need for better, safer, and more sustainable energy storage solutions. This work focuses on the use of covalent organic frameworks, a type of organic polymers, as electrode materials for lithium-ion batteries. First, the focus was on the synthesis and characterization of redox-active COFs, as well as the design of new COFs with expected increased conductivity. Afterward, the synthesized materials were used as electrodes in coin-cell type lithium batteries. For that purpose, the electrode preparation process was optimized, and the batteries were manufactured and tested. Thus, uncovering relations between covalent organic frameworks and their application as electrode materials for energy storage devices.

Table of Contents

List of Figures

List of Tables

Nomenclature

Symbols

C	Concentration of lithium ions	mol/m^3,
D	Lithium-ion diffusion coefficient	m^2/s
E	Energy density	J/kg
F	Faraday's constant	C/mol
I	Current intensity	A
M_w	Molar mass of the active material	kg/mol
n	Number of electrons	-
q	Charge	$A \cdot s$
Q	Specific capacity	$A \cdot s/kg$
Q_{Chg}	Charge specific capacity	$A \cdot s/kg$
Q_{DChg}	Discharge specific capacity	$A \cdot h/kg$
Q_{theo}	Theoretical capacity	$A \cdot h/kg$
R	Ideal gas constant	$J/mol \cdot K$
R_S	Solution resistance	$\mathrm{O}hm$ (Ω)
R_{ct}	Charge transfer resistance	$\mathrm{O}hm$ (Ω)
t	Time	s
T	Temperature	K
V_{oc}	Open-circuit voltage	V
V_{op}	Operating voltage	V
σ	Warburg coefficient	-
ω	Frequency	s^{-1}

Abbreviations

2D	Two-dimensional
3D	Three-dimensional
AQ	Anthraquinone
BET	Brunauer–Emmett–Teller
CE	Coulombic efficiency
Chg	Charge
COF	Covalent Organic Framework
CPE	Constant phase element

CV	Cyclic voltammetry
DAAQ	2,6-diaminoanthraquinone
DABH	1,4-dihydroxybenzene dihydrochloride
DABQ	2,5-diamino 1,4-benzoquinone
DChg	Discharge
DMAc	*N*,*N*-Dimethylacetamide
DMF	*N*,*N*-dimethylformamide
EDS	Energy-dispersive X-ray spectroscopy
FTIR-ATR	Fourier transform infrared spectroscopy- Attenuated total reflectance
LIB	Lithium ion battery
LUMO	Lowest unoccupied molecular orbital
NMP	N-methyl-2-pyrrolidinone
OCV	Open-circuit voltage
OEM	Organic electrode material
PEIS	Potentiostatic Electrochemical Impedance Spectroscopy
PVDF	Polyvinylidene fluoride
PXRD	Powder X-ray diffraction
TFP	Triformylphloroglucinol
TGA	Thermogravimetric analysis
TTF	Tetrathiafulvalene
TXM	Soft X-ray Transmission Microscopy

1. Introduction

Energy consumption keeps increasing every year, and whilst environmental issues such as global warming are at the forefront of the world's priorities, the energy sector still accounts for 60 % of the total greenhouse gas emissions.[1] Therefore, it is of major urgency to accelerate the energy transition from fossil fuels to cleaner energy sources.

Renewable energy sources, such as wind, solar, and hydropower, are at the forefront of this energy transition. Their share in the global energy supply keeps increasing, reaching 27% in 2019 and 29% in 2020, and an increased growth in the next years is predicted. Nevertheless, the use of this type of energy source is faced with a key hold-up, its intermittent availability. To fully utilize variable renewable energy sources and take full advantage of their potential, efficient energy storage solutions are essential. As a result, an expected 56% increase in storage capacity installed globally is forecasted for 2026. [1,2]

Energy storage technologies involve the transformation of one form of energy into another and can be classified into several types, such as electrochemical, mechanical, electrical, thermal, and chemical. Within the electrochemical category, one of the most well-known technologies is the lithium-ion battery. This type of rechargeable battery is among the most promising energy storage devices due to its high energy and power densities and is widely used in portable electronic devices, electric cars, and small-scale distributed energy systems. [3]

At present, in the European Union, lithium-ion batteries (LIBs) constitute the majority of projects in the electrochemical energy storage category. Emphasis is placed on the importance of increased efficiency and lifetime, as well as improved recyclability. [3,4]

The research and development of these batteries must focus on improving energy efficiency and safety while establishing as a priority the use and implementation of sustainable methods and materials. It is crucial to prevent what is projected to be a better solution from creating additional problems.

Currently, positive electrodes (cathodes) of commercial lithium-ion batteries are based on transition-metal oxides, whose energy density is limited by the specific capacity of these materials. [5] Moreover, the usage of these materials also raises environmental and ethical concerns, especially, but not exclusively, related to the mining conditions of some of these transition metals, such as cobalt. [6]

A promising alternative relies on the usage of electroactive organic materials to build organic electrodes. These materials consist mostly of elements abundant in nature, such as carbon,

hydrogen, oxygen, nitrogen, and sulfur, providing not only better availability of resources but also a more environmentally friendly solution. Additionally, the vast variety of diverse compounds as well as their structural tunability to fit specific applications, provide enhanced design flexibility for new organic electrode materials [7,8]

The idea to use organic electrode materials is not new and has been studied since the 1960s. However, the motivation to explore these materials as electrode materials decreased around the 1990s due to the successful commercialization of conventional lithium-ion batteries developed by SONY. Nonetheless, as society became increasingly more focused on sustainability issues, especially regarding energy, research into organic electrode materials had a big resurgence around 2008.[8]

Despite all the promising aspects of organic electrodes, these materials still face some challenges to offer a competitive alternative to conventional inorganic electrodes. The main limitations of organic electrodes are the low intrinsic conductivity and high solubility in the electrolyte (decreasing the cycling stability of the batteries). [8,9]

In the past few years, Covalent Organic Frameworks (COFs) have emerged as promising electrode materials to address the limitations associated with conventional organic materials. COFs are crystalline porous polymers linked by strong covalent bonds and characterized by their porosity, high stability, as well as structural tunability and chemical versatility. [5]

COFs show additional advantages in comparison to conventional organic materials towards their use as electrodes in LIBs. Namely, the higher stability and insolubility of the material in the electrolyte and the porosity which can facilitate the ion diffusion through the ordered channels improving the ionic conductivity. The challenge associated with low intrinsic electronic conductivity is still present in COFs, but it can be addressed using design strategies that take full advantage of the framework tunability. [5]

1.1.Objectives

Considering the promising nature of redox-active covalent organic frameworks (COFs), this work aims to explore and further the understanding of COFs used as electrodes in lithium-ion batteries (LIBs), as well as to design and synthesize new COFs with improved electronic properties for energy storage applications.

To accomplish the main aim of this dissertation, specific objectives were established such as:

- The synthesis and characterization of two redox-active COFs, already reported in the literature and tested as cathodes in LIBs, which have been used as reference. The positive electrode (cathode) preparation, manufacture of lithium metal half-cells using the COFs

as the positive electrode and the electrochemical testing of the batteries. This objective is crucial to understanding and optimizing the different procedures, techniques, and methodologies used in these fields.

- The study of the homogeneity of COFs with different thicknesses at different charging points using Soft X-ray Transmission Microscopy (TXM) at ALBA synchrotron (in collaboration with Andrea Sorrentino). This type of characterization using COFs as electrodes in LIBs is lacking in the current literature and is important to better understand the behavior of the COFs as electrodes, especially the relationships between morphology, particle size, and capacity.
- The design and synthesis of a new redox-active COF with expected increased conductivity.

1.2.Guideline

The chapters that make up this dissertation document are arranged as follows.

Chapter 2 presents a brief contextualization of the operation principles and key parameters of electrochemical cells as well as a deeper understanding of the specific case of lithium-ion batteries and in particular the current state of the art of cathode technologies.

Chapter 3 starts by introducing covalent organic frameworks, their structure, general properties, and common design strategies. Followed by a deeper reflection on why this type of organic polymers offers a promising solution for organic electrodes and the specific strategies used for this application.

Chapter 4 describes in detail all the materials and methods used. It is divided into two main sections that followed the previous structure of the document as well as the workflow used. The first section exposes the methods and materials used to synthesize and characterize covalent organic frameworks. The section follows the techniques and approaches used for the electrode preparation as well as for the electrochemical cell assembly and testing.

Chapter 5 follows the same structure as the previous chapter and exposes the results obtained in each section as well as a detailed discussion of the results. It correlates the results obtained for the electrochemical cells with the covalent organic frameworks used as the active material for the positive electrode and further discusses their relation.

Chapter 6 uncovers relations, conclusions, and learning points found during the analysis of the results and reflects on future work possibilities.

2. Batteries and Electrochemical Cells

This chapter will introduce the reader to fundamental information about batteries, and more specifically lithium-ion batteries. It includes a contextualization of the working operation principles of electrochemical cells followed by a contextualization of lithium-ion batteries' history and their key characterization parameters. In the end, the focus is narrowed to the positive electrode (cathode) and particularly to the field of organic electrodes.

Batteries are devices that through their electrochemical cell units convert chemical energy into electrical energy by using oxidation-reduction (redox) reactions, which involve the exchange of electrons between two species. [10]

The electrochemical cells and the batteries can be classified into the following two main categories.

- Primary cells or batteries are (mostly) irreversible, meaning that once they transform all the stored chemical energy into electrical energy, they are not able to recharge again easily and efficiently. As a result, they are discarded after only one use/discharge. They have high energy densities and provide an instant source of energy; they are also easily portable due to their lightweight and high availability because of their low price. [11]
- Secondary cells or batteries can be recharged, which means that after the cells are discharged it is possible to restore the cell to its charged state if electrical energy is provided to the cell. Moreover, compared to primary batteries, the energy density is usually lower but with a relatively high-power density and discharge rate. [11]

2.1.Working Principles and Operation

The basic electrochemical unit that converts chemical energy into electric energy is called an electrochemical cell. In addition, a battery involves the electrical connection of one or more cells, arranged in parallel or series, depending on the desired properties such as the operating voltage. [10]

The configuration of an electrochemical cell can be deconstructed into the following components:

- Positive electrode: the electrode with higher potential.
- Negative electrode: the electrode with lower potential.
- Electrolyte: an ion conductor substance, that allows the movement of ions between the two electrodes. Besides its good ionic conductivity, the electrolyte should not be electronically conductive to avoid a short circuit of the cell. It is most common for the electrolyte to be in liquid form however there are an increased number of gel-type and

solid electrolytes available. It is also important that the material is not reactive with the electrode materials and that it proves to be stable under cell operation conditions. [10]

- Separator: a permeable membrane that physically separates the two electrodes but is permeable to the electrolyte, permitting the transfer of the ions and maintaining the ionic conductivity. [10]

The two electrodes can also be named according to the electrochemical reaction as cathode or anodes. [11]

- Anode: where an oxidation reaction takes place accompanied by the loss of electrons to the circuit. This way, the electrode is oxidized and behaves as the reducing agent.
- Cathode: where a reduction reaction takes place accompanied by the gain of electrons from the external circuit. Thus, the electrode is reduced and behaves as an oxidizing agent.

It is important to note that in rechargeable/secondary cells, these terms are not synonyms for the positive and negative electrodes. A positive electrode can be a cathode or anode depending on the two possible cell operation states, charge or discharge, which can be described as follows [3,11]:

- Discharge: the cell stored energy is being used. The cell voltage decreases, this is the potential difference between the electrodes decreases. Electrons flow from the negative electrode, where an oxidation reaction is taking place, to the positive electrode, which is consequently reduced with the gain of electrons. Thus, in this situation, the negative electrode is an anode, and the positive electrode is a cathode. Furthermore, the operation is completed with the flow of cations in the same direction as the electrons' flow, from the negative to the positive electrode, and with the opposite flow direction of the anions.
- Charge: as the cell is connected to a power supply, the current flows in a reversed direction. The cell voltage increases and the electrons flow from the positive electrode, where oxidation takes place, to the negative electrode which gains electrons and is reduced. In this way, the positive electrode is now the anode, and the negative electrode is the cathode. The cations will also follow the flow of the electrons and go from the positive to the negative electrode. [10]

The oxidation-reduction (redox) reactions occur at the active sites of the electrode materials and can be represented by the following reaction equations:

$$aA + ne^- \rightleftharpoons bB \quad (1)$$

$$cC - ne^- \rightleftharpoons dD \quad (2)$$

$$aA + cC \rightleftharpoons bB + dD \quad (3)$$

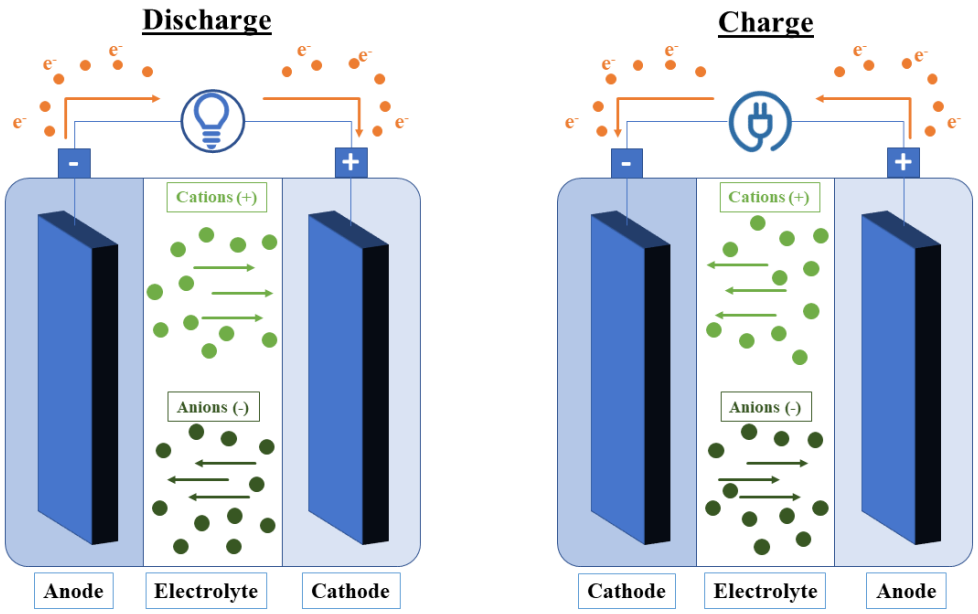

Figure 1: Schematic representation of the discharging (left) and charging (right) processes in an electrochemical cell. Adapted from [5,10]

The reduction reaction is represented by Equation 1, where the molecules of component A gain n electrons from the molecules of B. This way, A is reduced and acts as an oxidizing agent. On the other hand, Equation 2 represents the oxidation reaction where the molecules of C lose n electrons to the molecules of D. Thus, C is oxidized and acts as a reducing agent. The combination of the two half-cell reactions represents the overall reaction and is exemplified by Equation 3. [11]

2.2. Key parameters

Electrochemical cells are complex systems that can be described and characterized by different parameters. In this section, the parameters of greatest interest for the purpose of this project will be highlighted.

2.2.1. Energy Density

The amount of energy stored ($W \cdot h$), by weight or volume, in a cell is designated as energy density. It can be classified as volumetric energy density ($W \cdot h/L$) when defined per volume or as gravimetric energy density ($W \cdot h/kg$) when compared to the weight of the cell.

The energy density (E) is determined by discharging the cell while using a suitable current and it can be calculated by multiplying the operating voltage in volt, represented with V_{op}, by the specific capacity, either by weight ($A \cdot h/kg$) or volume ($A \cdot h/L$), represented with Q_{DChg}, as expressed through Equation 4. [11]

$$E = V_{op} \times Q_{DChg} \quad (4)$$

- Capacity (Q)

The cell capacity is a measurement of how much electricity the active materials of the electrodes can produce and is defined in ampere-hour. The specific capacity is defined as a function of the weight of active material in the electrode ($A \cdot h/kg$). [10]

The theoretical capacity of a particular active material depends only on the materials' properties and can be calculated, assuming 100% conversion of the active material, using the Faraday's law of electrolysis, represented in Equation 5. [11–13]

$$Q_{theo} = \frac{n \cdot F}{3600 \cdot \frac{M_w}{1000}} = 26{,}8 \times \frac{n}{M_w} \quad (5)$$

Here, F represents Faraday's constant of $96485\ C/mol$; M_w is the molar mass of the active material in g/mol; n corresponds to the number of electrons implicated in the redox reaction (oxidation or reduction) of the active material.

On the other hand, the specific capacity, Q, obtained through the cell charge and discharge is calculated by dividing the capacity obtained by the mass of active material in the electrode, in $A \cdot h/kg$ or equivalent.

- Voltage

Fundamentally, the term voltage can be defined as an electric potential difference between two points, in this case, the positive and negative electrode, that enables the movement of electrons. The voltage acts as the driving force of the electrochemical cell. However, when studying batteries, it is possible to encounter several different voltage parameters that must be distinguished, such as:

  - Theoretical voltage: can be obtained experimentally under standard conditions or calculated using free-energy data. Its value depends on the materials of the electrodes, as well as other factors such as temperature and electrolyte.
  - Open-circuit voltage: represented as V_{OC}, is the voltage when the battery is under no external load or power source, in other words, when no electric current is going through the circuit.
  - Working or operating voltage: measured when an electric current is flowing out of the battery, meaning that the cell is connected to an external electrical load and is discharging. The usual voltage range that a battery experiences while being discharged.
  - Cutoff or end voltage: represents the voltage at the end point of the discharge.

2.2.2. Charge and discharge parameters

As the batteries are subjected to subsequent charge and discharge processes, it is important to use specific parameters that allow the analysis of the performance of the battery during this cycling process.

- C-rate and Rate Performance

The charge and discharge rate, abbreviated as the C-rate, is a parameter used to convey the current used during discharge (or charge). Thus, the C-rate is related to the maximum capacity and gauges how quickly a battery is discharged. A C-rate of mC can be interpreted as the cell discharging (or charging) completely in $\frac{1}{m}$ hours. [11]

To determine the multiples or fractions of the C-rate needed to charge a cell with a specific current or to find the current needed for a specific C-rate, it is possible to use Equation 6 [10]:

$$I = m\, C_{rate} \cdot Q \tag{6}$$

Here, m corresponds to the multiple of the C-rate; I is the discharge or charge current in ampere (A) and Q is the capacity of the cell in ampere-hours ($A \cdot h$). This way, for a cell with a capacity of 50 $A \cdot h$ at a rate of $2C$, the discharge current is 100 A, while at 1 C is 50 A and at $C/2$ is 25 A.

Nevertheless, it is not viable to use any intended C-Rate since above a certain limit the increased rate causes a decrease in the maximum capacity. Thus, the rate performance of the battery is limited. [14]

Some of the battery parameters that influence rate performance are the electronic conductivity of the electrodes, the ion diffusion both in the electrolyte and in the electrode, and the reactions occurring inside the battery. Additionally, to influence these parameters and improve rate performance some possible optimizations to the electrode consist in the increase of the material porosity and the decrease of thickness and particle size. [14]

- Coulombic Efficiency

Once a cell has been charged and discharged, it means it has completed a full cycle. For each cycle, the ratio of the discharge and charge capacity corresponds to the coulombic efficiency in percentage, represented in Equation 7.

$$CE\ (\%) = \frac{Q_{DChg}}{Q_{Chg}} \times 100 \tag{7}$$

The Coulombic efficiency gives information about the released cell capacity in one cycle and, therefore, about the cycle charge efficiency since it relates the energy taken out from the battery to the energy added to it. [15]

2.2.3. Cycle Life

When thinking about the lifespan of a cell or battery, there are two different terms to take into consideration. One is the definition of calendar life which corresponds to the total time a cell can remain operational, and it includes not just the time the cell is in use but also being stored.

The cycle life, on the other hand, is equal to the total number of charge-discharge cycles that a battery may go through before losing 80 % of its rated capacity."[11]

Here, it is important to note that several different factors can contribute to loss of capacity and greatly decrease the cycle life of the cell. For instance, impurities or even active material getting dissolved in the electrolyte; the deterioration of the morphological structure of the electrodes; corrosion of the electrodes; and unexpected and unintended chemical reactions.

In addition, there is another cell phenomenon that can contribute to capacity loss and increased cell resistance, named the passivation layer or the solid electrolyte interphase (SEI). It is defined as a layer between the electrode and the electrolyte as soon as the first discharge, but that keeps growing with the following cycles up to several nanometers in thickness. The irreversible loss of capacity, especially during the first cycle originates from the incorporation of lithium into the solid electrolyte interphase [10,11,16]

However, interestingly, the passivation layer does not only contribute negatively to the cell but also has a crucial role in maintaining the cell electrochemical stability, through the prevention of unwanted reactions between the electrode and the electrolyte while still being conductive to the ions, but acting as an electronic insulator. [17]

2.2.4. Internal Resistance

There are two different types of cell resistance that are important for the study of electrochemical cells.

First, we must consider the electrical resistance (or resistivity) that opposes the electric current; this is the flow of electrons through the cell. Inversely proportionally, it is possible to define the conductivity (intrinsic property) or conductance (extrinsic property) as a measure of how well a material conducts electric current. The cell's cycle life, as well as rate performance, will be better when the internal resistance is lower, and the electrical conductivity is higher. [1]

As the transport of electrons faces resistance, the transport and flow of ions also do face resistance. This resistance can be found both in the electrolyte and in the electrodes, as well as at its interface. This way, it is important to take into consideration this resistance to ion transport as well as the inverse parameter, the ionic conductivity, defined as the easiness of ion flow through the cell. [11]

2.3. Lithium Ion-Batteries

One of the most notorious types of batteries is the rechargeable lithium-ion battery, due to the crucial role it previously had in enabling the mobile revolution and currently being in the forefront of vehicle electrification. Owing to their high energy and power densities they are responsible for powering many small portable electronics, such as mobile phones and computers, as well as electric vehicles. [3,11]

The history of the invention of the lithium-ion battery starts with Alessandro Volta in 1800 with the creation of the galvanic or voltaic cell and was slowly built through the achievements and knowledge of many scientists.

Lithium is especially interesting for battery applications due to several different particularities, namely, the fact that lithium is the lightest metal, with low molecular weight and density. Additionally, its electronic configuration, $1s^2 2s^1$, characterized by just one valence electron, makes it easier for lithium to lose electrons and become positive. Lastly, its high specific capacity, 3860 $mAhg^{-1}$, and high electrochemical potential, -3.04 V against H_2/H^+, make it a good material for high energy density batteries. Nevertheless, lithium's extremely high reactivity with air, water, and nitrogen made it a difficult material to work with and a challenge to create an operational battery. [11,18]

It was in 1958 due to William S. Harris' work that a different number of non-aqueous electrolytes, such as propylene carbonate, were identified to work well for electrochemical applications with lithium metal and permitted the first commercialization of primary lithium batteries.[11,19]

The following research focused mainly on materials of interest to be used as positive electrodes since it was anticipated that lithium metal should be used as the negative electrode. In 1965, Walter Rüdorff showed that titanium disulfide (TiS_2), a metal chalcogenide of the MX_2 type, could host lithium ions due to its layered structure with binding sites. This material allows chemical intercalation, so the reversible process of introduction and extraction of lithium ions into the layered material maintains its structural integrity. [11,19]

The focus towards the use of this type of materials continued and M. Stanley Whittingham and colleagues demonstrated lithium intercalation in Li_xTiS_2, as well as other materials, and their potential as electrodes. This was followed, in 1976 at Exxon, by the demonstration and

commercial development of a rechargeable battery using TiS_2 as the positive electrode and lithium metal as the negative electrode. [19]

Unfortunately, this commercial progress was interrupted due to the high reactivity of lithium metal, since during the recharging process occurred the formation of dendrites in the metal surface of the lithium. These dendrites can be especially dangerous since they could grow enough to penetrate through the battery, including through the separator, and reach the positive electrode, which could cause a short circuit and potentially evolve into danger of explosion.[19]

Considering these dangers, research shifted away from the use of lithium metal and focused on the idea that both electrodes could use intercalation materials to accommodate lithium ions using a cell configuration based on ion transfer, also known as "rocking chair" cells, whose principle had already been previously demonstrated.

Around 1980, at Oxford University, Goodenough and colleagues found another intercalated material, Li_xCoO_2, that could be used as a positive electrode and would make possible the use of materials in the negative electrode with higher potentials. [19]

Following this discovery, in 1985 at Asahi Kasei Corporation, Akira Yoshino discovered that petroleum coke, a carbonaceous material, had the ability to accommodate a significant number of lithium ions, whilst having a low enough potential difference with Li/Li^+ and being stable under operating conditions.

Using petroleum coke as the anode and Li_xCoO_2 as the cathode, Yoshino developed an operational rechargeable lithium-ion battery that when tested for damages would not originate explosions or fires. All these discoveries culminated in 1991 with the first production and commercialization of the rechargeable lithium-ion battery, by the Sony Corporation.[19]

Ultimately, due to their discoveries related to the development of the lithium-ion battery, Akira Yoshino, John B. Goodenough, and M. Stanley Whittingham were awarded the 2019 Nobel Prize in Chemistry.[19]

These groundbreaking and significant findings did not mark the end of the lithium-ion battery's development; instead, numerous advances and improvements have since been reported.

2.3.1. Positive electrode overview

For a material to be considered for application as a positive electrode in a LIB it must fulfill several requirements. First, the material must have a useful working voltage, this is, high voltage in respect to the lithium metal potential in addition to being able to incorporate lithium ions into its structure in a reversible way and have a good lithium diffusivity. Besides, it should be stable with the electrolyte and insoluble in it, as well as, have a high electronic conductivity. [10]

The active materials currently used more as positive electrodes can either be a metal oxide or a metal phosphate. These materials can be further classified into three different categories according to their structure: rock salt or layered; spinel and polyanion or olivine. It should be noted, that all three different types of structures were reported as interesting positive electrode materials by John Goodenough's research group.[20]

Table 1: Summary of the current most used inorganic cathode chemistries as well as key characterization parameters for each material. Adapted from [10,21]

Name abbreviation	Material	Structure	Specific Capacity (mAh/g)	Midpoint Voltage (V vs Li)
LCO	$LiCoO_2$	Layered	155	3,9
LMO	$LiMn_2O_4$	Spinel	100-120	4,05
LMNO	$LiNi_{0.5}Mn_{1.5}O_4$	Spinel	130	4,6
LFP	$LiFePO_4$	Olivine	160	3,45
NMC	$LiNi_{1-x-y}Mn_xCo_yO_2$	Layered	140-180	3,8
NCA	$LiNi_{0.8}Co_{0.15}Al_{0.05}O_2$	Layered	200	3,73

As shown in Table 1, most of the materials currently used for positive electrodes are based on transition metals such as cobalt (Co), manganese (Mn), and nickel (Ni). These materials face some limitations for the energy density improvement of the batteries. Furthermore, there is also a raised concern around resources availability and cost around the value chain, as well as some environmental and ethical concerns, particularly related to the mining of these materials.[6,22]

2.3.2. Organic electrodes for LIBs

A promising alternative to these inorganic materials is the use of organic electrode materials (OEMs). This idea is not new and can be traced back to 1960, but organic electrodes received less attention around 1990 due to the fast and successful development of transition metal oxides as positive electrodes. However, due to the environmental concerns raised around the inorganic materials, the idea of organic electrodes had a big revival around 2008. [8]

Organic electrodes pose a good solution for these sustainability issues since these materials consist of elements that are abundant in nature, such as carbon, hydrogen, oxygen, nitrogen, and sulfur, and the materials themselves can be obtained from compounds present in nature or through biomass. Additionally, organic electrode materials have enhanced design flexibility due to the number of diverse compounds available and their structural tunability. [7,8]

The first example of organic electrodes for lithium-ion batteries was reported in 1969 when some carbonyl compounds were used as positive electrodes. However, this type of material is soluble in aprotic electrolytes, which results in a fast loss of battery capacity. Since this study, a lot of different compounds were explored such as conductive polymers, organosulfur and nitrile compounds, organic compounds, and more recently imine and azo compounds. [8]

One of the positive and interesting characteristics of most organic electrodes, in comparison with their inorganic counterparts, is that when undergoing redox reactions, the structure of the compound doesn't go through major changes and often just has small bond rearrangement. Additionally, it is often easier to adopt these organic materials to different types of batteries since the redox reactions are not bound to the type and charge of the ions.

It is possible to divide different types of organic electrode materials into three different categories, namely, n-type, p-type, or, bipolar type, according to their redox reactions and mechanisms. The n-type compounds, including carbonyl, nitrile, imine, and azo compounds, first undergo reduction, and during the redox reaction, they go from neutral to a negatively charged state. Due to their low redox potentials, they are usually used as the negative electrode. On the other hand, p-type, including some organosulfur compounds, conjugated N-heterocycles, and nitroxyl radical, first experience oxidation, and to remain electroneutral, they need to establish a connection with anions from the electrolyte. These compounds are usually employed as positive electrodes due to their high redox potentials. The kinetics of their redox reactions are typically fast, but since the majority of their weight does not have redox sites and not all sites that exist are used, the resulting capacity is limited. [8]

Currently, the most promising solution, between the compounds presented, is the use of n-type compounds as positive electrodes. However, these and other organic electrode materials still face some design and application challenges and limitations such as the low electronic conductivity and the stability when in contact with non-aqueous electrolytes.

Nevertheless, there is a new class of porous organic polymers that recently emerged as a new promising electrode material for energy storage applications, namely Covalent Organic Frameworks (COFs). The next chapter will go deeper into this class of materials and explain why they are regarded as an interesting alternative.

3. Covalent Organic Frameworks

This research field emerged in the year 2005, when Adrien P. Côte, Omar M. Yaghi, and co-workers, reported for the first time the successful design and synthesis of a crystalline and porous covalent organic framework.[23]

3.1.Structure and Properties

Covalent organic frameworks (COFs) are highly ordered, crystalline porous organic polymers linked through strong covalent bonds and using building blocks that are composed mainly of light elements such as carbon, hydrogen, oxygen, boron, and nitrogen. [23,24]

Furthermore, COFs offer enhanced design opportunities to fit specific properties and application needs because of the vast possibility of organic compounds that can be used as initial building blocks allowing design flexibility and tunable functionality. [2]

Additionally, the robust structure frameworks and strong covalent bonds provide high chemical and thermal stability to the materials while the reversible reaction that creates the frameworks allows, through error correction and structural rearrangement, the formation of the crystalline structure instead of an amorphous material. [25,26] In general, there is an inverse relationship between crystallinity and stability. Covalent bonds based on reversible reactions normally lead to high crystallinity and, in some cases, to lower stability. When the reversibility of a reaction is high, it allows the rearrangement of the structure to its thermodynamic minimum which translates to a material with higher crystallinity. However, the same high reversibility harms the COF stability since the break of the bond is the reverse of its formation.[26]

The extended framework that characterizes COFs, is composed of two key elements that will be further discussed, namely the building blocks or linkers, terms used to describe organic functionalized molecules or monomers; and the linkages, the type of bonds formed through the connection of the building blocks.[25] The geometry of the extended framework is predefined by the properties of these building blocks, as well as their size, connectivity, and symmetry. This allows for high precision control over the special assembly of the framework, allowing the synthesis of two-dimensional (2D) or three-dimensional (3D) COFs depending on the COF geometry.[27]

Two-dimensional (2D) COFs, consist of 2D sheets of the linked COF stacked through π– π interactions. Due to the COF porosity and the stacking, a layered structure with periodically aligned channels is formed. On the other hand, 3D COFs structures have their networks expanded

into one more dimension, usually due to the use of building blocks with sp^3 orbital hybridization, using for example carbon, boron, or silane atoms. [28]

3.2.Linkage Types

COFs can be characterized considering the type of linkage that connects the different building blocks, that in turn are related to the different types of reactions available for the synthesis of these frameworks.[26]

The first COF was synthesized through a condensation reaction and incorporated used boronic acid anhydride and boronic ester. [23] Using boroxine and boronate-ester linkages was appealing because the reactions have extremely high reversibility that allows the synthesis of materials with high crystallinity. However, the COFs were also highly susceptible to hydrolysis under mild and ambient conditions due to this high reversibility; reducing the applicability of the material.[26]

Following this discovery, a lot of different reactions and types of linkages were studied to tackle this stability and crystallinity problem, including hydrazone, azine, and imide linkages, as well as other linkage types. Two interesting linkage types that will be further explored are the imine linkages, the current most popular linkage, and the β-ketoenamine linkage. [26,27]

3.2.1. Imine Linkage

To form an imine linkage, an amine reacts with an aldehyde usually through Schiff base reactions (Figure 2). These condensation reactions are usually enabled by the use of a catalyst, commonly an organic or Lewis acid. [24,27]

The stability of the material does not depend only on the type of reaction and linkage but also on the type of building blocks. However, imine-based COFs have overall high stability. Additionally, when an aromatic amine reacts with an aromatic aldehyde, there is further stabilization around the 2D COF layers through π-system conjugation, displaying moderate electron stability and consequently enhanced electrical conductivity. [27,29]

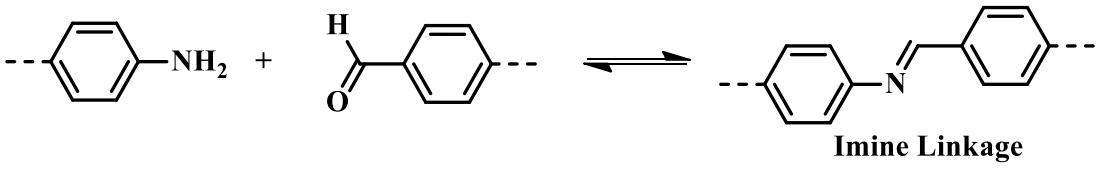

Figure 2: Representation of imine linkage formation.[27]

3.2.2. *β*-ketoenamine linkage

Another type of linkage exhibiting higher stability is the *β*-ketoenamine linkage. COFs containing this type of linkage are known to maintain their structural integrity and porosity even in the presence of strong acid and bases. [25,27]

The high COF stability is due to its specific synthesis mechanisms also using an aldehyde and an amine, represented in Figure 3. First, the building blocks go through a reversible Schiff base reaction, where an imine linkage is formed, and the COF is in enol form with bonded hydroxyl groups. It is this highly reversible reaction that allows the formation of a crystalline structure, due to the building blocks being able to arrange according to the most thermodynamically favorable structure and being able to do error correction and defect healing in the structure. Finally, the COF enol form goes through an irreversible enol-keto-tautomerization reaction, creating the *β*-ketoenamine linkage and further chemically stabilizing the structure and network of the COF.[27]

This strategy synthesis was first reported in 2012 by Banerjee and colleagues, where 1,3,5-triformylphloroglucinol (TFP), which is characterized by formyl groups next to hydroxyl groups, was used as the aldehyde building block to react with different amines. [30] The high stability in acidic conditions of *β*-ketoenamine linkages, led other researchers to explore this type of reaction for specific applications such as electrochemical energy storage (due to the linkage stability in the acidic electrolyte). [31]

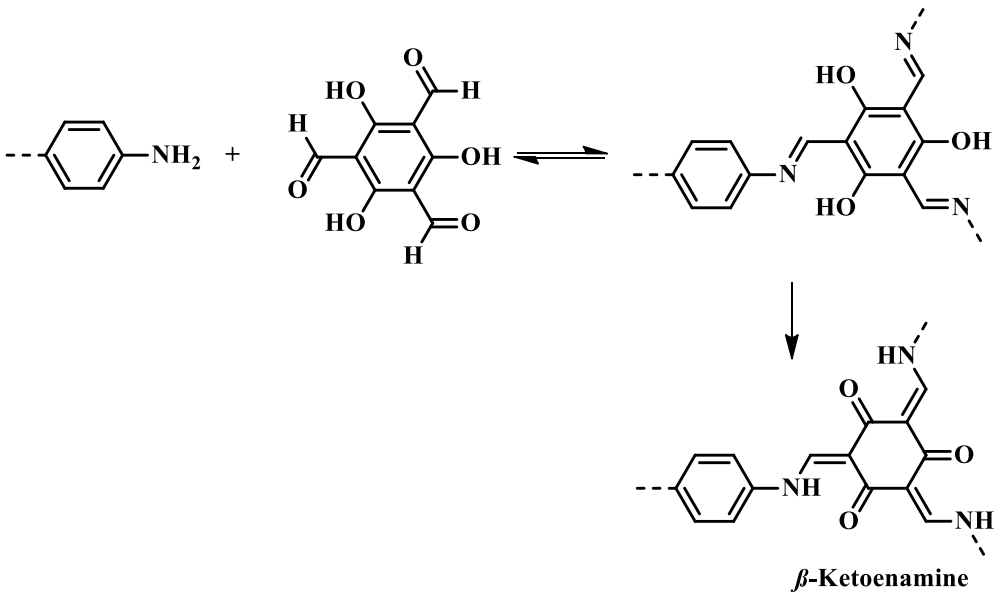

Figure 3: Synthesis process of a β-ketoenamine linkage. The first step consists of a reversable Schiff base reaction, where an imine linkage is formed followed by an irreversible enol-keto-tautomerization.[27]

3.3.Design Principles

There are different possible strategies to design new COFs, taking into account the different design goals.

One of these strategies is the topological design, where a targeted topology is first chosen and then deconstructed into its geometric units that can subsequently be found in different organic molecules. Later, it is crucial to study and identify the synthetic conditions that can yield a crystalline structure using the chosen organic building blocks. The design process is illustrated in Figure 4. [25] To simplify, usually, this type of design concept can be represented through the basic geometry representation of the active sites' relative position to each other. Figure 5 shows some topology examples and the corresponding linker geometries. [24,27]

This design strategy is only possible because the organic building blocks maintain their initial geometry during the COF synthesis. It is also easier to predict a smaller number of possible expected structures using the hypothesis that it is more likely to obtain the most symmetric structures, this is called the symmetry hypothesis. [32]

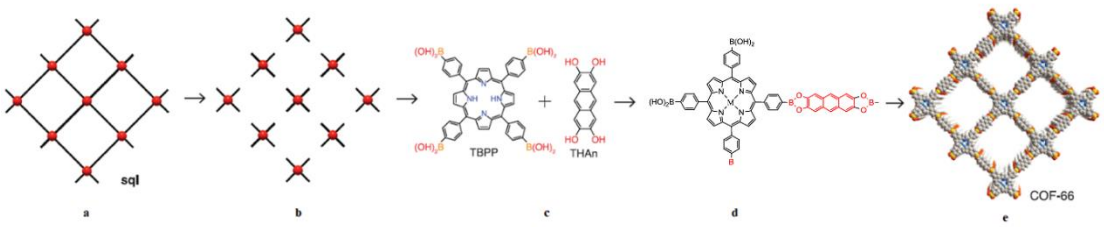

Figure 4: a) Chosen target topology, based on a sql tetragonal net. b) Fundamental geometric units of the structure, corresponding to (in this case) 90º angles. c) Equivalent geometric units in organic molecules, combining a linker with the 90º angle. Adapted from [25].

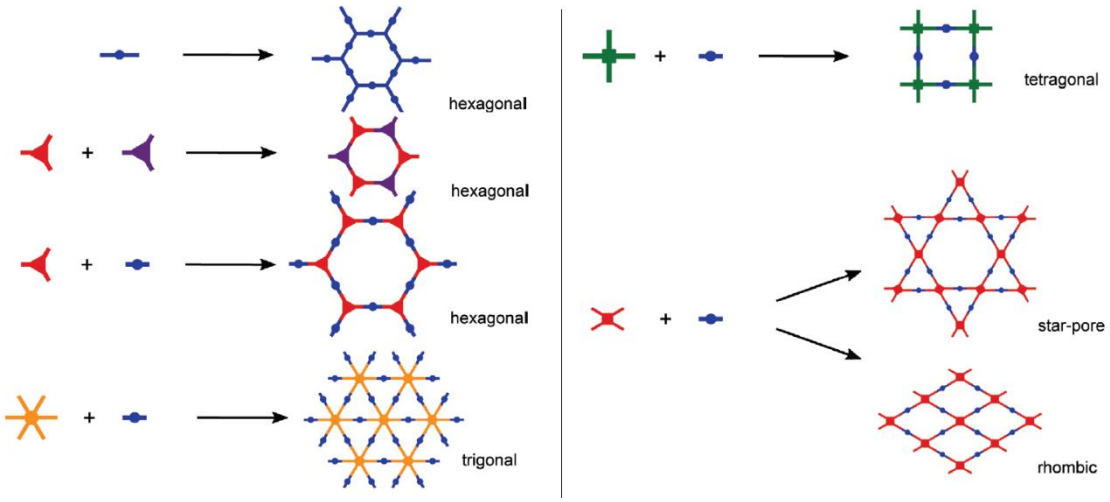

Figure 5: Examples of topology patterns created using common linker geometries used for 2D COFs.[27]

Other design strategies focus on the need for a specific property useful for a targeted application. This process of tailoring the design according to the targeted function of the material is designated as functionalization and can be implemented in two different situations: pre-synthesis by choosing adequate building blocks or carrying functionalization processes in these molecules; or post-synthesis through the modification of the COF framework, possible mainly due to the porous structure and highly stable structure. The double feasibility of the frameworks' functionalization enables increased flexibility in the design process as well as the possibility of highly tunable materials with higher performances. [25]

These design strategies coupled with the intrinsic porosity and ordered structure of COFs, allow the design of novel COFs with useful properties for a variety of different purposes, including electrochemical energy storage applications.

3.4.COFs as electrode materials

Covalent organic frameworks have emerged as promising materials for application in electrochemical energy storage due to their high chemical and structural versatility.

For the specific application as electrodes in metal-ion batteries, it is crucial the design of a framework using redox-active building blocks being able to undergo oxidation and reduction reactions, so the material will be able to fulfill the basic premise of electron transfer. The charge and discharge processes of an electrochemical cell depends on the availability of these redox sites in the materials framework. [24]

When the use of organic electrode materials was discussed, it was highlighted the challenge to achieve cycling stability due to the high solubility of these materials in the electrolyte. Polymerization was presented as an efficient solution for this problem but raised another issue that would render the material less useful. Since the linear polymers tend to twist and loop within themselves, most of the redox-active sites were not accessible, making it difficult to achieve high performance with this material. Moreover, COFs present the stability advantages of an organic polymer but also have the enhanced benefit of higher accessibility to its redox sites due to the highly ordered porous structure. [8,33]

As previously, explained in the second chapter, lithium-ion batteries don't involve just the transfer of electrons but also the transport of lithium ions from one electrode to the other. Here, the intrinsic porosity of COFs as well as the high alignment of those pores, offer an opportunity for the storage and diffusion of the lithium ions. [24]

Moreover, the design strategies of COFs for electrode applications are focused on the improvement of the conduction of the electrons, the electronic conductivity, and the improvement

of ion diffusion. It is, however, important to not disregard other properties that influence the overall performance of the material for its electrode function. To better optimize the design of these materials it is crucial to understand the connections between the COF structure and its performance as an electrode material.[33]

3.4.1. Structure-Performance relationship

To better access this connection between the structure of the COF and the performance of the electrode, it is important to retrieve the concepts described as key parameters of lithium-ion batteries in Chapter 2 and connect them with the structure of the material. The key parameters that will be specifically discussed are the voltage, capacity, cycle life, and rate performance.

- Voltage

The molecular structure, mostly the redox-active site linkages, is the parameter that has more influence on the COF electrode voltage.

Considering the different redox reactions and mechanisms, COFs can also be divided into the same three different categories used for conventional organic electrode materials, namely, n-type, p-type, or, bipolar type, as previously described in Chapter 2. The n-type COFs are associated with lower redox potentials and are subsequently lower voltage and thus are more propitious to be used as the negative electrode. On the other hand, p-type COFs involve the change between a neutral and positive state and are linked with higher redox potentials and thus higher voltage being subsequently typically used as the positive electrode. [33]

- Capacity

The theoretical capacity of a material is directly proportional to the number of electrons transferred per molecule and inversely proportional to the molecular weight (Equation 5, Chapter 2). Moreover, it can be inferred that it is possible to improve the COFs' theoretical capacity using building blocks with a lower molecular weight and whose redox reactions allow an increase in the number of transferred electrons per molecular weight. Additionally, the more active sites the COF has the higher the capacity, this way, the capacity of the material is increased if all linkages in the COF are redox-active. [33]

However, the full theoretical capacity of the material cannot be achieved when the battery is in operation, leading to the need to discuss the factors that influence the actual practical capacity. First, the practical capacity is influenced by the electrical and ionic conductivity of the COF material, since the higher the flow of electrons and ions, the higher the achievable capacity. Furthermore, the accessibility of the redox-active sites is another crucial parameter. When the COF layers are stacked too close to each other, the percentage of active materials buried and not

accessible for reaction tends to be higher, highlighting the importance of the material's thickness, the particle and pore size, and surface area. Some of the strategies that can be used to improve these parameters are the post-synthetic exfoliation of bulk COFs or the direct synthesis of COF thin films. [28,33]

- Cycle life

The cycle life is decreased, for example, by side reactions of the active materials and high solubility of the active materials in the electrolyte, a big concern in organic electrodes that is improved in COFs due to the robust and highly stable porous frameworks.

However, even though the previously stated is true it does not mean that all COFs have the same degree of stability when in contact with the electrolyte. Here, different types of COF linkages can be connected to different cycling performances, for example, some COFs with imine or β-ketoenamine linkages showed some material decomposition during cycling and consequentially lower cycling stability. Here, exfoliation of the materials can also improve its performance through the improved stability of reaction intermediates and the higher surface contact of the COF's active material. [33]

- Rate performance

As previously explained in Chapter 2, the rate performance is directly connected with the electronic and ion conductivity.

The ionic conductivity is facilitated with the use of COFs due to the intrinsic highly ordered porous frameworks. However, as previously stated, the porous channels in 2D COFs can sometimes be compromised due to the strong π-π interactions and too closely stacked COF layers, leading to a more sluggish ion diffusion than first anticipated. This can be improved with COF exfoliation or the use of COF thin films, leading to more accessible porous channels and consequently to easier and faster ion diffusion. [12,28,33]

It is also crucial to increase the eletronic conductivity of COFs, through the careful choice of building blocks and COF linkages, or their combination with materials with enhanced conductivity, such as conductive polymers, graphene, and carbon nanotubes. [34]

In a nutshell, it is crucial to carefully choose the COF building blocks as well as the functionalization strategies. For the COF to be used as electrode material it is important to ensure high stability of the structure, to prevent decomposition and unwanted reactions. As well as guarantee highly structured pore channels for an efficient ion diffusion and increased accessibility to the redox-active sites. Along with high electrical conductivity for a better transfer of electrons.

3.4.2. Enhanced electrical conductivity strategies

The importance of the improvement of the COFs' electrical conductivity has been reiterated in the previous sections of this chapter. Here, will be highlighted possible strategies used for this purpose.

The electrical conductivity in 2D COFs is influenced by the COF structure and is highly dependable on π-π stacking of the COF layers, this is, the "through-space" electron mobility utilizing the noncovalent interactions. On the other hand, the charge mobility also happens through the covalent linkage of the materials, called a "through-bond" mobility, and is dependent on in-plane π-conjugation. [28,29]

Since the electrical conductivity in the COF layers increases through electron delocalization and in-plane π-conjugation, it is important to carefully choose the COF linkages to enhance these properties. As was highlighted before, imines present a moderate delocalization and are considered a good alternative for conductive COFs. [29]

Since both in-plane π-conjugation and π-π stacking of the COF highly depend on the electronic intrinsic properties of the building blocks used, it is extremely important to carefully select which building blocks will be used and combined.

There are a lot of different types of building blocks with interesting electronic properties, two with special interest will be highlighted.

- **Quinone**

The properties displayed by redox-active quinone building blocks are especially interesting for electrochemical applications due to their large theoretical capacity, stability, and reversibility. As well as the possibility of tunable molecular properties due to the enabled easier functionalization. [29]

  - Anthraquinone (AQ)

The use of anthraquinone (AQ) derivatives as a building block for organic electrode applications, has been previously reported [35,36], as well as, as used as a COF building block for the same application. [12,13,31] This application is possible due to the good electrochemical properties and the electron-acceptor behavior can be explained by the low-lying LUMO found mostly in the benzoquinone ring. [29]

Additionally, the anthraquinone can have three different redox states (neutral, radical anion, and dianion) formed through two consecutive redox processes, involving one electron each, as illustrated in Figure 6.

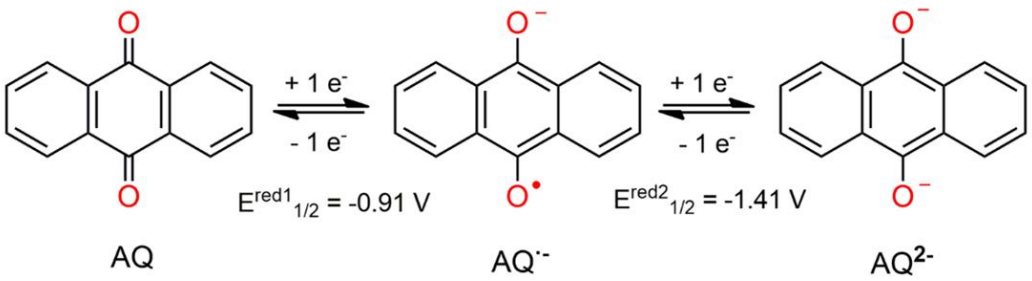

Figure 6: Schematic representation of the anthraquinone redox processes.[29]

- Benzoquinone and hydroquinone

Benzoquinones have some of the same advantages and exhibit interesting electrochemical properties. The redox processes also include reversible redox reactions involving one electron each, while forming a semiquinone radical. [37] The reduction of hydroquinone and the oxidation of hydroquinone don't just work as good prospects for electrochemical applications but are also known to have an important role in biological redox processes. [38]

The flexible functionalization of the quinoid ring with a lot of different groups, open the doors for the usage of these linkers across the different application. The rigid π-conjugated structure further establishes these quinones as good electroactive building blocks. [37,38]

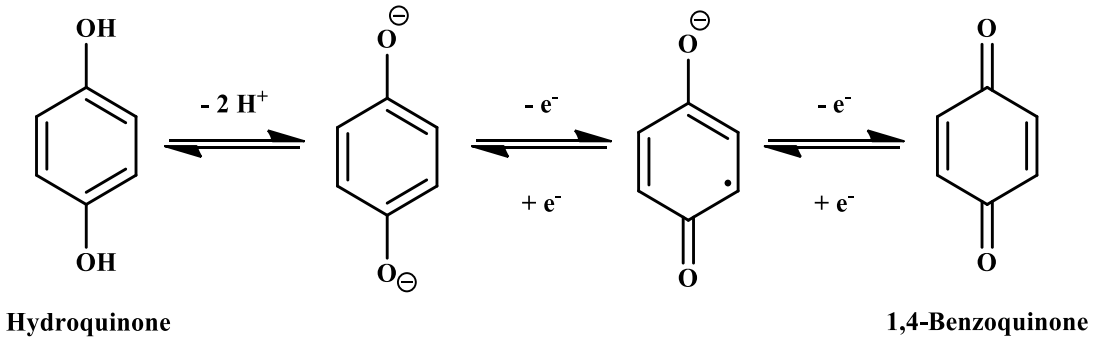

Figure 7: Schematic representation of hydroquinone redox processes.[38]

- **Tetrathiafulvalene (TTF)**

Contrary to the quinones previously described, tetrathiafulvalene (TTF) and its derivatives are known to be excellent electron-donor compounds. Thanks to this factor and also due to their excellent redox properties, TTF building blocks work for a panoply of different electronic applications.

The relatively low potentials of the reversible oxidation of TTF into $TTF^{\cdot+}$ and TTF^{2+}, illustrated in Figure 8, as well as the affinity to electron donation, occur because of the high-lying HOMO energy level. Additionally, TTF structures also offer the possibility of high functional flexibility

and the frameworks enhanced charge-transport efficiency through the development of π-π stacking with short S-S interactions, enabling the synthesis of COFs with higher intrinsic electrical conductivity. [29]

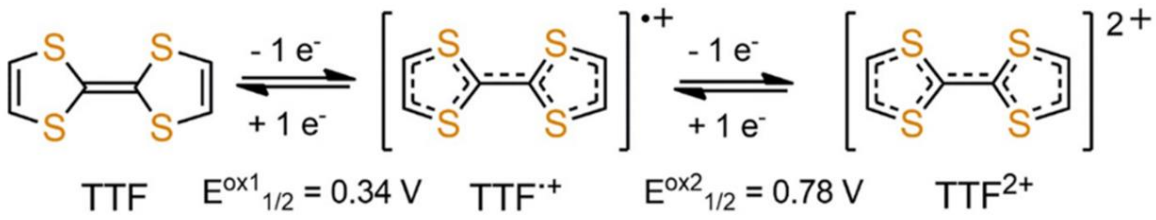

Figure 8: Schematic representation if the TTF redox processes, showing the different redox states and potentials [39]

3.5.Synthetic Methodologies

The syntheses of covalent organic frameworks require the reaction through multiple sites and the formation of reversible covalent bonds, to allow the self-healing processes and error correction as the framework is built. [24]

Even though the most used synthetic method is solvothermal synthesis, several different techniques have been proven useful for different applications. These syntheses methods will be briefly described.

- Solvothermal synthesis

The reaction building blocks, as well as solvents and a catalyst, are joined in a closed vial and heated at a certain temperature during a specific reaction time. The reactivity of the building blocks as well as their solubility in the selected solvents is of extreme importance. Furthermore, the parameters that needed to be optimized when looking into a new synthesis using this method for the preparation of crystalline porous frameworks are the solvents and their proportion, catalyst, temperature, and reaction time. One of the biggest drawbacks of this technique is the long reaction times usually needed to yield crystalline COFs [24,27]

- Microwave-Assisted Synthesis

This technique allows faster reaction times and was explored to offer an alternative to the long reaction times of the solvothermal synthesis. The general process consists in first joining the building blocks with a suitable solvent in a closed microwave tube while under a nitrogen or vacuum atmosphere. The tube is then heated at a specific temperature and stirred for a short time (from a few minutes to up to an hour). [24,27]

- Ionothermal Synthesis

This technique uses ionic liquids as the solvent, catalyst, and template for the formation of solid structures. The applicability of this technique is extremely reduced due to the very high temperatures required.

- Mechanochemical Synthesis

This technique surged to simplify the synthesis process. Here, the COFs are formed simply by grinding the building blocks at room temperature using a mortar and pestle. It is also possible to enhance the reaction rate using liquid-assisted grinding where a small catalyst solution is added to the process. The resulting COFs usually have equivalent chemical stability but lower crystalline when compared to other techniques. [24,27]

- Sonochemical Synthesis

This technique uses ultrasound and allows shorter reaction times. The chemical reaction is accelerated due to the higher local temperatures and pressure, created due to the cavitation process devised from the bubble formation and collapse process. [24,27]

3.6.Post-synthetic exfoliation of bulk COFs

The post-synthetic exfoliation of bulk COFs has an important role when designing COF as electrode materials. This exfoliation to yield few-layer COF nanosheets can also be described as a top-down synthesis process. The goal of this process is to break the stacking between the different layers of the 2D COFs forming a nanosheet material. [28] The most common techniques used for exfoliation can be divided into the following strategies:

- Mechanical exfoliation/delamination

These strategies do not require the use of any solvents and are achieved through simple techniques. The most common methods are the use of a mortar and pestle or ball mining, where the ball mill is more reproducible due to the automated operation. However, the scotch tape method, popularized by graphene, has been also explored. The major limitation of these techniques is related to the lack of control over the thickness of the COF nanosheets created. Since most COFs materials are bulk powders and not large crystals, it is often not ideal to use this method for their exfoliation. [40]

- Liquid-assisted exfoliation

The disintegration of the bulk layer connections is achieved in the liquid phase using the application of an external energy source (mechanical force), such as sonication. It is important to

choose an appropriate solvent and to optimize the sonication parameters, such as the power, temperature, and time. Such requirements as well as common low exfoliation yields make this a difficult approach. A subtype of this technique includes the chemical exfoliation of 2D COFs by reducing the interlayer interaction through the introduction of intercalated molecules or groups. Additionally, it is also possible to have other specific molecules such as surfactants to further prevent the re-aggregation of the layers. Due to this, the chemical exfoliation methods are more efficient but still complex to optimize. [28,40]

4. Materials and Methods

This chapter will be divided into two major parts, a first section focused on the materials and methods used for the synthesis and characterization of the covalent organic framework materials; and a second section focus on the techniques used for the electrochemical cell assembly and testing using the materials synthetized in the first section.

4.1.Covalent Organic Frameworks

First, two different COFs were synthetized and characterized using different building blocks, employing procedures already reported in the literature. Later, it was also attempted, the design and synthesis of a new COF material.

4.1.1. Synthesis

All the synthesis procedures used the solvothermal technique, where the building blocks were added to a Pyrex vial with the corresponding solvents and catalyst. The vial charged with all the components is first tightly sealed and then heated during a specific amount of time. After the end of the reaction time, the resulting material is washed with appropriate solvents that dissolve the building blocks but do not interfere with the COF structure. Finally, the resultant COF is dried at an appropriate temperature that can evaporate the solvents used without damaging the material.

- **DAAQ-TFP-COF**

For the synthesis of the DAAQ-TFP-COF, a reported procedure was followed[12,31] using 34 mg of 2,6-diaminoanthraquinone, DAAQ (0,143 mmol), and 20 mg of 1,3,5-triformylphloroglucinol, TFP (0,0952 mmol), as the building blocks. The solvents *N*,*N*-Dimethylacetamide (DMAc) (0,9 mL) and mesitylene (0,3 mL) were added to the vial that was sonicated at room temperature for a few minutes, until the visible dissolution of the monomers in the solvent mixture. Lastly, 50 µL of acetic acid 6M was added to the mixture. The Pyrex vial was then tightly closed and heated in an oven at 120 °C for 3 days.

The dark red powder obtained from the synthesis was filtrated and washed using *N*,*N*-dimethylformamide (DMF) to remove any unreacted starting material until no color was observed in the filtrate, followed by a final wash with acetone. The material was then dried at 180 °C for 24 hours resulting in a dark red powder that was weighted and characterized by different techniques.

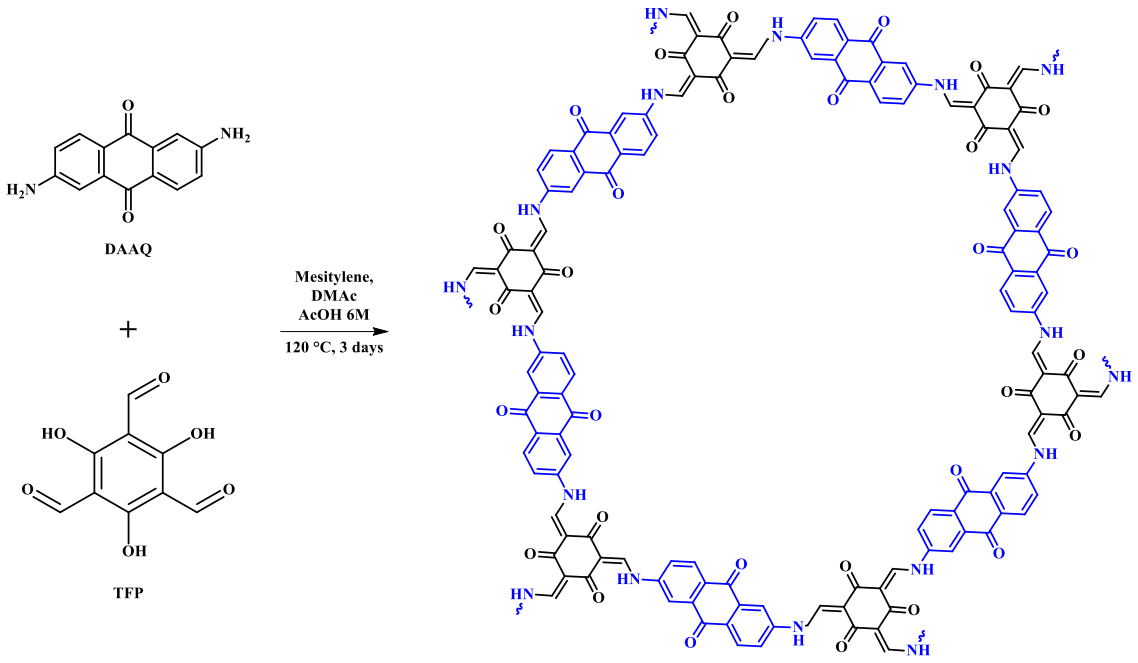

Figure 9: Schematic representation of the synthesis of DAAQ-TFP-COF.

- **DABQ-TFP-COF**

For the synthesis of the DABQ-TFP-COF, a reported procedure was also followed[12] and TFP was again used as building block. The intention is to substitute the DAAQ building block with 2,5-diamino 1,4-benzoquinone (DABQ) since it is a molecule with lower molecular weight which should translate to a resulting COF with higher theoretical specific capacity but maintaining the same topology and stability. However, the direct synthesis of this COF does not produce crystalline structures. To overcome this limitation, the synthesis process is divided into two reactions. The first reaction is the condensation of 2,5-diamino 1,4-dihydroxybenzene dihydrochloride (DABH) and TFP to obtain DABH-TFP-COF (Figure 10). Then the post-synthetic modification of DABH-TFP-COF through an oxidation reaction with triethylamine yields DABQ-TFP-COF. [12]

- <u>Condensation Reaction</u>

30 mg of DABH (0,141 mmol), 20 mg of TFP (0,0952 mmol), 0,6 mL of DMAc and 0,6 mL of mesitylene were mixed in a Pyrex vial. The mixture was sonicated at room temperature for a few minutes, until the visible dissolution of the solid materials in the solvent mixture and 50 µL of acetic acid 6M were added to the mixture. The Pyrex vial was then tightly sealed and heated at 120 °C for 3 days.

The powder obtained from the synthesis has a dark black color and was filtrated and washed using DMF, until no color is observed in the filtrate, followed by a final wash with acetone. It was then dried at 120 °C for 24 hours. The resulting black powder was weighted and characterized.

- Oxidation Reaction

50 mg of the DABH-TFP-COF, obtained in the previous reaction, were dissolved in 5 mL of triethylamine. The suspension was stirred at room temperature and under air atmosphere and left stirring overnight. The resulting material was then filtrated and washed with tetrahydrofuran (THF), acetone and ethanol. The resulting black powder was then dried at 60 °C for approximately 5 hours.

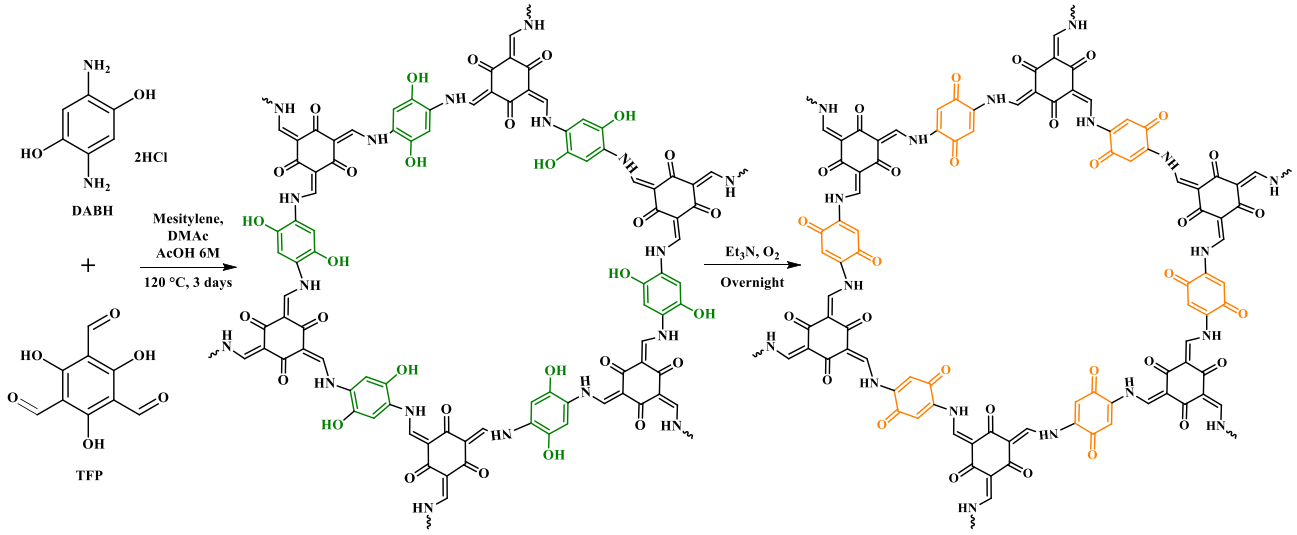

Figure 10: Schematic representation of the synthesis of DABQ-TFP-COF.

- **TTF-DABQ-COF**

The synthesis of TTF-DABQ-COF differs from the other two since it has never been reported before. The goal of the design of this material is to combine a compound with high capacity, DABQ, with another with expected high intrinsic electronic conductivity, a TTF-derived compound with four benzaldehyde groups attached to it, designated as TTF-Ph-TA.

As it was done with the DABQ-TFP-COF, the reaction here was also designed to be conducted in two separate steps. First, a condensation reaction between DABH and TTF-Ph-TA, where the aldehyde groups of the benzaldehyde groups in the TTF-Ph-TA were expected to react with the amine groups of the DABH, creating an imine linkage (C=N).

The synthesis technique chosen was solvothermal synthesis since it is the most common technique for the synthesis of imine-linked COFs. The parameters that need to be optimized for the reaction to yield crystalline COFs are the following: the solvents used and their proportion, the type of catalyst used, temperature, and reaction time. The parameters should be changed one by one until the optimal reaction conditions are obtained. As initial conditions, the parameters were derived through the synthesis procedure of similar COF synthesis reported in the literature[41,42]. So first, 13,6 mg of TTF-Ph-TA (0,0219 mmol) and 9,6 mg of DABH (0,0451 mmol) were mixed

with 0,5 mL of dioxane; 0,5 mL of mesitylene and 0,1 mL of acetic acid 3M as the modulator (achieving an overall proportion of 1:5:5 v/v). The Pyrex vial containing the reaction mixture was sonicated for a few minutes, then tightly sealed, and left in the oven for 3 days at 120 °C.

Before the washing of the obtained black precipitate, solubility tests were done to guarantee that the linkers, TTF-Ph-TA and DABH were well dissolved in the chosen washing solvents. The black precipitate with a flake consistency was then washed with THF, acetonitrile and acetone and left to dry at 70 °C overnight. To keep optimizing the reaction conditions, the strategy used was to change one parameter at a time. The first parameter to modulate was the type of solvents used

4.1.2. Characterization

Once the COFs were obtained through the synthesis mentioned before, it was crucial to characterize well the material obtained using the following techniques:

- Fourier transform infrared spectroscopy- Attenuated total reflectance (FTIR-ATR)

This characterization technique was used to analyze the chemical structure of the synthesized COF, through the analysis of the detected functional groups. It is especially useful to confirm if the wanted COF linkage was formed, and to check for the disappearance of functional groups from the building blocks or other non-interesting structures.

- Powder X-ray diffraction (PXRD)

Powder X-ray diffraction (PXRD) is used to determine the crystalline structure of the COF samples. First, it is inferred from the PXRD patterns if the structure is crystalline through the presence of defined intense peaks. Then, it is checked if the peaks correspond to the ones expected through the use of simulated PXRD patterns obtained from theoretical models for the particular COF being studied. Finally, is possible to correlate the different peaks with the different sets of interplanar planes (hkl) and calculate the different interplanar distances, making it possible to determine, for example, the pore diameter of COFs or the stacking distance.

- Scanning electron microscopy (SEM)

This technique allows for a morphology and surface analysis of the obtained COF materials, as well as chemical mapping and composition by energy-dispersive X-ray spectroscopy (EDS).

- Thermogravimetric analysis (TGA)

The thermogravimetric analysis is done under a nitrogen atmosphere and using a heating rate of 5°C/min from 20°C to 600°C. Tests were done both with and without pre-heating of the samples, and it was found that this step is crucial to ensure the total evaporation of solvents from

the COF structure. This technique displays the weight variations of the material as it is subjected to higher temperatures, making it especially useful to evaluate the thermal stability.[43]

- Cyclic voltammetry (CV) [44]

Cyclic voltammetry tests were used to study the electrochemical processes associated with the COFs and their building blocks. The methods used can be divided into two different procedures. The CV tests of the organic building blocks are done in solution since the compounds are highly soluble in the electrolyte solution. On the other hand, COFs are insoluble in this electrolyte solution and the CV characterization had to be done differently. In this case, one day before the electrochemical testing, the COF was dissolved in a binder solution of 1,4 mL ethanol and 0,5 mL nafion (3:1 v/v relation of ethanol to nafion) and subsequently applied drop by drop using a micropipette into the center of the glassy carbon working electrode and left to dry at least overnight. The process of deposition of the binder with COF solution can be repeated, once the solvent evaporates, until a satisfactory thickness of COF onto the electrode is achieved.

The closed vessel used for cyclic voltammetry is also called an electrochemical cell and three different electrodes were used during our tests in a potentiostat. A silver wire was used as the reference electrode and platinum and glassy carbon were used as the counter and working electrodes, respectively. The electrolyte solution was prepared by dissolving 800 mg of trabutylammonium hexafluorophosphate into 20 mL of acetonitrile. The salt, also called supporting electrolyte, is used to decrease the solution resistance.

Once the electrochemical cell is connected to the respective wires, the cyclic voltammetry tests can start. Here, it was important to carefully choose the upper and lower potential limits according to the materials being tested. Additionally, tests using different scan rates were used, usually between 0,1 and 0,5 V/s. To finalize the test, a small quantity of ferrocene is added to the electrolyte solution as reference and a voltammogram is recorded. The ferrocene test is done to be used as an internal standard and reference.

- Gas adsorption

The nitrogen isotherm adsorption of the DAAQ-TFP-COF was measured through a collaboration with Prof. Felix Zamora from the Universidad Autónoma de Madrid (UAM). Using this technique, it is possible to calculate the BET surface area, an important parameter for the characterization of the COF's porosity.

4.2.Electrochemical Half Cell

Once the DAAQ-TFP-COF was well characterized the next goal consisted of the preparation of electrodes using the COF as active material, followed by the assembly of electrochemical cells, in this case, a half cell. Furthermore, the cells went through several different electrochemical tests to properly test their performance and mechanisms as well as the ultimate performance of the DAAQ-TFP-COF as a positive electrode.

4.2.1. Electrode preparation

The first step consisted of mixing the active material, DAAQ-TFP-COF, with conductive carbon black and the polyvinylidene fluoride binder (PVDF), using a weight ratio of 6:3:1, respectively. This weight ratio followed the values reported in the literature for this material. [12,13] A step that was found to be crucial, through the optimization of this process, was the need slowly grind the solid materials with a mortar and pestle.

The next step involved the addition of a solvent, in this case N-methyl-2-pyrrolidinone (NMP) to properly mix the materials and achieve the mixture slurry consistency needed for the deposition of the material. This is one of the trickiest steps in electrode preparation since it is difficult to specify an exact quantity of NMP needed. The strategy used was to initially calculate the NMP needed to achieve a 20% w/v, with the solids previously weighted, and to slowly keep adding NMP drops until a satisfactory slurry consistency was achieved.

The slurry was then mixed for 2 to 4 hours until a homogenous slurry mixture with the pretended consistency was achieved.

Next, the slurry mixture was spread into the current collector, in this case, aluminum foil coated with carbon black. This was the current collector used since our electrode material will be used as the positive electrode. The casting was done using a tape and blade technique, where the aluminum foil was taped on both sides into a nonconductive plastic surface using two layers of commercial large scotch tape, allowing an area of aluminum foil adequate to the quantity of slurry prepared. The slurry is then dropped into the aluminum foil and subsequently carefully spread using a blade or spatula.

Once the slurry deposition is finished, the coated aluminum sheet was left to dry over a hot plate at 60 °C for a few hours or until the material is not shiny. Finally, the coated aluminum foil was dried overnight under vacuum at 120 °C to remove the NMP.

A visual representation of this processes can be consulted in the Appendix A.4.

4.2.2. Half-cell assembly

For the studying and testing of the electrochemical performance of the DAAQ-TFP-COF as a positive electrode material, a half-cell configuration was used with lithium metal as the counter and reference electrode.

The CR2032 coin-cells were the type of electrochemical cells chosen for this study. Furthermore, it was important to first establish the electrodes and separator diameters considering the cell type limitation. The separator needs to have the highest diameter to avoid possible short circuits and to ensure a high area of contact with the electrodes. Thus, the diameters chosen were 10 mm for the negative electrode, the lithium metal; 12 mm for the positive electrode, the DAAQ-TFP-COF composite; and 16 mm for the separator, using a cellulose-based which is DuPont's proprietary material. These characteristics are summarized in Table 2.

Table 2: Summary of the material and diameter used for the positive and negative electrodes as well as the separator.

Component	Material	Diameter
Positive electrode	DAAQ-TFP-COF	12 mm
Separator	Cellulose-based (DuPont's proprietary material)	16 mm
Negative electrode	Lithium metal	10 mm

Assembly of the half coin cells was done inside a glove box with constant monitoring of the oxygen and water levels, considering their high reactivity with the lithium metal being used. The direction of the assembly was from the negative case to the positive case, as illustrated in Figure 11, and special care was taken to carefully align all the parts.

The liquid electrolyte used was 1,0 M $LiPF_6$ in EC/DMC=50/50 (v/v), battery grade, a lithium hexafluorophosphate solution in ethylene carbonate and dimethyl carbonate. For the electrolyte deposition, a micropipette was used to carefully deposit 50 µL drop by drop on top of the separator while making sure it covered all its surface.

Finally, after the complete assembly, the cell was closed using an automatic pressure crimping machine

A schematic illustration of the half-cell components is represented in Figure 11 and a photography representation can be consulted in the Appendix A.5.

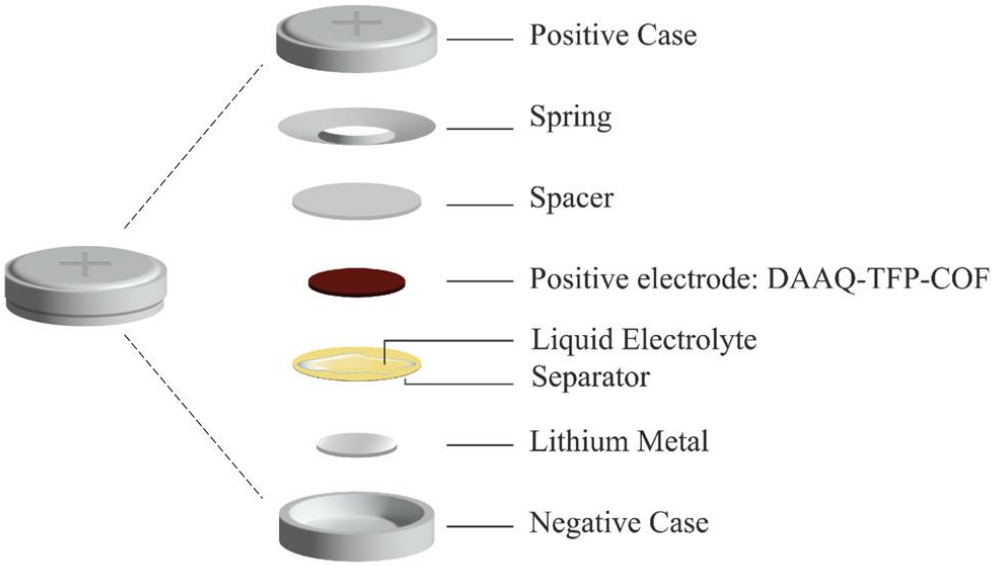

Figure 11: Schematic representation of the electrochemical half-cell components with the assembly structure used.

4.2.3. Half-cell Testing

After the cells were assembled, the first test consisted of the measure of the open-circuit voltage (OCV) using a multimeter. The measure of OCV was done several times during the electrochemical testing process, to ensure that the cells still had a useful potential difference.

After the first OCV measure, the cells were left to rest for at least a few hours but ideally for up to a couple of days. Once the cells were ready for further electrochemical testing, the tests were done in the order they are mentioned in this section. Additionally, it is important to mention that all the cells were done under ambient temperature and that small plastic bags were used around the coin-cells during the tests to act as electrical insulators and prevent short-circuiting or other damage.

- Potentiostatic Electrochemical Impedance Spectroscopy (PEIS)

The impedance tests were done using a frequency range of 0,1 Hz to 10^6 Hz and voltage amplitude of 10 mV. Further processing of the obtained data was done using the EC Lab software.

Using, PEIS data it is also possible to determine the lithium-ion diffusion coefficient (cm^2/s) using Equation 8. This coefficient helps to understand the diffusion process of the ions through the structure.

$$D = 0{,}5\left(\frac{T \cdot R}{A \cdot n \cdot F^2 \cdot \sigma \cdot C}\right)^2 \quad (8)$$

Here, T represents the temperature (in Kelvin); R is the ideal gas constant ($8{,}314\ J/mol \cdot K$); A corresponds to the surface area of the interface between the electrolyte and the particles, in this

case, the area of the electrode; n is the involved number of electrons per molecule; F represents the Faraday's constant ($9{,}65 \cdot 10^4\ s \cdot A/mol$); C corresponds to the concentration of lithium ions (mol/cm^3), Li^+; and σ is the Warburg coefficient. [11,12]

The concentration of lithium ions (C) is calculated through the number of electrons moved during the first discharge of the cell, since for each electron transported there is an equivalent lithium-ion. First, the charge (q) associated with the discharge of the cell during the first cycle was calculated using Equation 9 where the current intensity (I) is multiplied by the time it took the cell to completely discharge.

$$q = I \times t \tag{9}$$

$$N = \frac{q}{1{,}6 \times 10^{-19}} \tag{10}$$

Then, the number of electrons is calculated through Equation 10 considering that each electron has a charge of $1{,}6 \times 10^{-19}\ C$. Finally, the number of moles was calculated taking into account that for each mole of electrons there are $6{,}02 \times 10^{23}$electrons and the resulting number is equal to the mole number of lithium ions. Through, this number of moles of the lithium ions, the concentration was calculated by diving this number by the corresponding area.

Furthermore, the Warburg coefficient, σ , was obtained using Equation 11, where σ corresponds to the slope when Z_{RE} is plotted against $\omega^{-0,5}$, for the lower frequency's values.

$$Z_{RE} = R_e + R_{ct} + \sigma \cdot \omega^{-0,5} \tag{11}$$

- Cyclic Voltammetry (CV)

For cyclic voltammetry characterization of the half-cells, the upper and lower potential limits were defined as 1,5 V and 3,5 V. The tests were done using different scan rates from 2 mV/s to 5mV/s.

- Cycling performance tests (Charge and Discharge cycle characterization)

Since the DAAQ-TFP-COF used as the positive electrode active material does not have lithium in its framework, the electrode should first be lithiated which means that the battery should first be discharged and that should be considered when programming the cycling test. Two different groups of cells were cycled using different conditions.

The first group of half-cells was cycled using constant charge and the electric current intensity was different for different cells and even changed along the cycling process for the same cell, the values varying from 10 to 50 µA.

The second group of cells was cycled with the same conditions, including the final number of cycles being the same and the current intensity being the same, 30 µA. The only difference between the cycling programs of the cells was that two were planned to finish the cycling in a charged state and the other two in a discharged state. In this case, the cycling program did not just include constant charge cycling but also included phases of constant voltage.

- Soft X-ray Transmission Microscopy (TXM)

This characterization technique was still not implemented during the writing of this thesis. However, some important steps were already taken. Four similar cells were cycled until they reached 50 cycles, being that two finished in a discharged state and the other two in a charged state, as previously described. These cells were then opened and the positive electrodes with the DAAQ-TFP-COF active material were extracted inside the glove box and stored in a safe container. They were then shipped to Doctor Andrea Sorrentino from the ALBA Synchrotron, to be further studied using Soft X-ray Transmission Microscopy (TXM).

Using Soft X-ray Transmission Microscopy (TXM) with ALBA's MISTRAL beamline, which allows an energy range of 270 eV to 1200 eV, it will be possible to study the X-ray absorption near edge structure (XANES) imaging at the O-K edge and perform a 2D mapping of the chemical states of the electrodes with DAAQ-TFP-COF as active material. Thus, it will be possible to visualize and analyze the special distribution of the different oxygen species and obtain information about the homogeneity of the state of charge within the electrode. Moreover, studying electrodes at different states of the charge and discharge cycle allows the study of the lithiation process of the electrodes using DAAQ-TFP-COF.

Additionally, it is intended to perform this study using COFs after an exfoliation process, with a total of 3 different thicknesses (including the bulk material), since it already established the influence of the material's thickness and its specific capacity. These results will help to further understand this relationship and establish connections between particle size, morphology and capacity.

5. Results and Discussion

This chapter follows the same structure division as previously used in Chapter 4. First, the results obtained through the synthesis and characterization of various covalent organic frameworks will be discussed. Then, the results related to the coin-cell assembly process and testing will be presented. Lastly, some insights that relate to the two sections will be explored.

5.1.Covalent Organic Frameworks

The results and discussion around the synthesis and characterization are presented for each COF synthesized.

5.1.1. DAAQ-TFP COF

The interest in using 2,6-diaminoanthraquinone, DAAQ, for the preparation of COFs to be used as an electrode material, is due to the high theoretical capacity of this organic compound, with a value of 151 $mA \cdot h/g$. Furthermore, when DAAQ is linked to 1,3,5-triformylphloroglucinol, TFP, the result is a highly stable COF connected through β-ketoenamine linkages. These linkages yield particularly stable and crystalline COFs as a result of the synthesis mechanisms being divided into two steps, as represented in Figure 12. First, the DAAQ and TFP building blocks go through a reversible Schiff base reaction, where an enol form of the COF is built and an imine linkage is formed. This reversible first step is crucial because it allows the structure to go through defect healing and error connection mechanisms that enable the COF's crystallinity. Next, β-ketoenamine linkages are formed due to an enol-keto-tautomerization reaction, an irreversible reaction that stabilizes the structure of the COF.

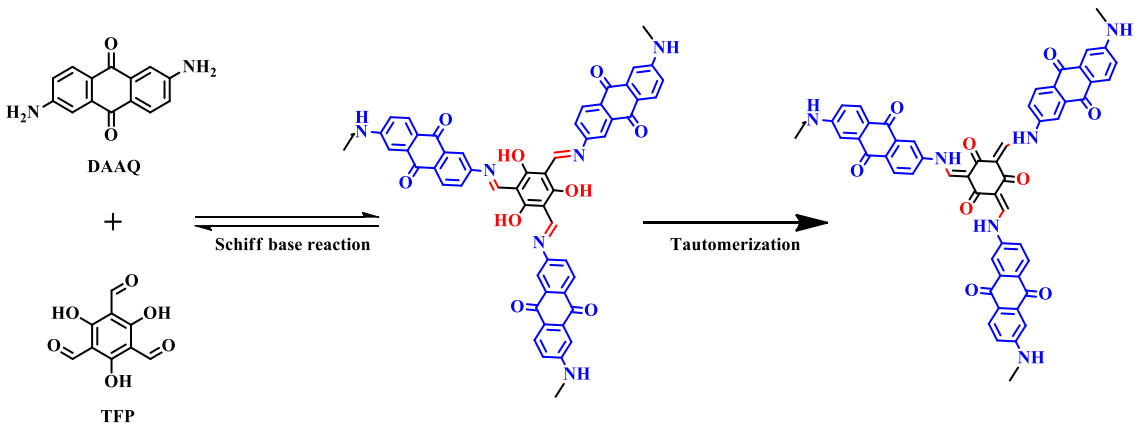

Figure 12: Two-step mechanism of the β-ketoenamine linkage reaction for DAAQ-TFP-COF. First, a Schiff base reaction yields an imine followed by an enol-keto-tautomerization.

To access the correct synthesis of the DAAQ-TFP-COF, the first characterization techniques used were the Fourier transform infrared spectroscopy with attenuated total reflectance (FTIR-ATR) and the Powder X-ray diffraction (PXRD).

First, the spectrum obtained from the FTIR analysis gives us crucial information about the chemical structure of our COF, Figure 13 (left). A visible band at 1250 cm^{-1}, indicates the presence of the C-N linkage associated with β-ketoenamines. Additionally, the disappearance of the N-H band from the amino groups, clearly present in the DAAQ precursor around from around 3300 to 3400 cm^{-1}, is another indication of the correct synthesis and washing of the material.

To access the crystallinity of the material, PXRD was used and the diffractogram was compared with one obtained through simulation, Figure 13 (right). The obtained diffractogram shows an intense diffraction peak at 3,4° associated with the (100) reflection lattice. This peak can relate to the diameter of the COF's pore determined as 2,60 nm, using the Bragg's Law equation. Additionally, a broad diffraction peak can be spotted at 26,9° at the (001) lattice associated with the stacking of the COF layer in a 2D dimension, allowing the determination of the distance between adjacent layers as 0,33 nm or 3,3 Å.

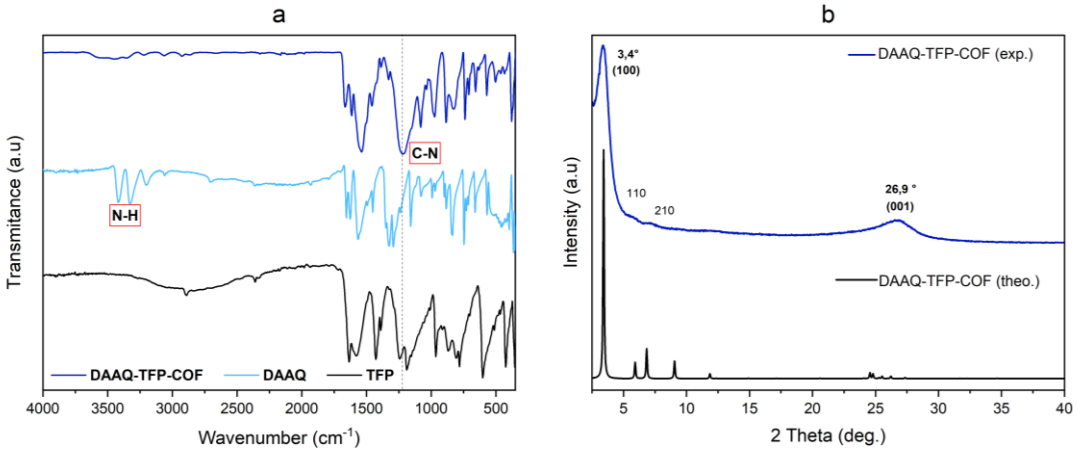

Figure 13: (a) FTIR-ATR spectra related to DAAQ-TFP-COF and its precursors, DAAQ and TFP.(b) Experimental and simulated diffractogram of DAAQ-TFP-COF.

The chemical structure and crystallinity analysis are then followed by the study of the thermal stability of the material, using thermogravimetric analysis (TGA). The obtained thermal decomposition profile can be found in Figure 14.

Through the study of the nitrogen adsorption isotherms, the BET surface area was determined to be $1407 \pm 6{,}483\ m^2/g$ with a molecular cross-sectional area of 0,1620 nm^2. This BET surface area is a good indication of the high porosity of the material.

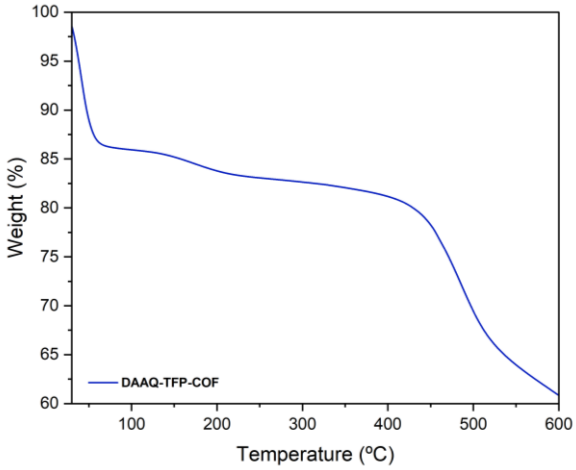

Figure 14: Thermogravimetric analysis (TGA) of DAAQ-TFP-COF.

Analyzing the thermal degradation profile, it is first visible a clear drop in weight even after the 100 °C. However, this weight loss is not necessarily related to the thermal stability of the material but to eventual residues present in the sample, for example, adsorbed solvents that were used during the washing of the material. This could be prevented by previously heating the sample until 150 °C, to ensure no residues when performing TGA.

Nevertheless, it can be said that DAAQ-TFP-COF is particularly stable until a degradation temperature of 420°C. Additionally, the material underwent only partial decomposition after the 600°C, since at the end of the test only 61% of the weight was lost, leaving residue that was not decomposed.

Next, cyclic voltammetry was performed to study the electron transfer processes, this is the oxidation and reduction processes of the COF. The resulting voltammogram is represented in Figure 15.

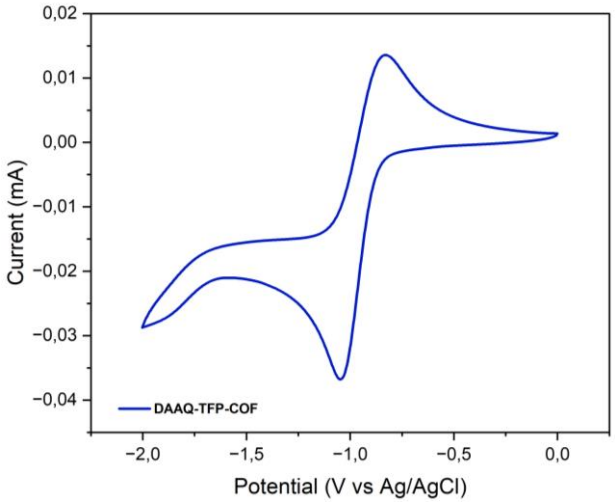

Figure 15: Cyclic voltammogram of DAAQ-TFP-COF.

The visible “duck” shape indicates the presence of reduction and oxidation. In this case, one oxidation peak at -0,83 V and one reduction peak at -1,0 V. The redox process is associated with the anthraquinone’s two-step reversible redox process, where anthraquinone is reduced to the respective radical anion and dianion, as represented in Figure 6, Chapter 3.

Lastly, using scanning electron microscope (SEM) with energy dispersive X-Ray spectroscopy (EDS) the morphology as well as the chemical composition of the COF could be accessed. The morphologically analysis of the sample by SEM shows particle sizes up to 100 µm. The elemental analysis by EDS obtained was 69,8 wt% of carbon, 21,52 wt.% of oxygen, and 8,59 wt.% of nitrogen, showing consistent results with what was theoretically expected, and the results found in the literature.[12] The images and all results obtained can be consulted in Appendix A.2

5.1.2. DABQ-TFP-COF

The interest in substituting 2,6-diaminoanthraquinone, DAAQ, as a linker, for 2,5-diamino 1,4-benzoquinone (DABQ) for the preparation of COFs to be used as an electrode material, is again, related with the theoretical capacity of this compound, 221 $mA \cdot h/g$, a value much higher than DAAQ. Since the capacity of an electrode’s material is crucial to its performance, it is expected that COFs using DABQ will translate into better electrode materials.

Since using DABQ directly as a building block with 1,3,5-triformylphloroglucinol, TFP, only yields amorphous materials, the standard synthesis procedure is divided into two reactions. The first reaction, the condensation of 2,5-diamino 1,4-dihydroxybenzene dihydrochloride (DABH) and TFP, where DABH-TFP-COF was obtained and characterized. The second reaction was the oxidation of DABH-TFP-COF to produce the intended DABQ-TFP-COF. [12]

- DABH-TFP-COF

The reaction of DABH and TFP, follows the same mechanisms as the reaction previously described for DAAQ-TFP-COF. This is, first DABH and TFP goes through a reversible Schiff base condensation reaction, that forms an imine linkage and allows the creation of a crystalline COF. Followed by an irreversible enol-keto-tautomerization reaction, creating the β-ketoenamine linkage that offers increased stability to the framework.

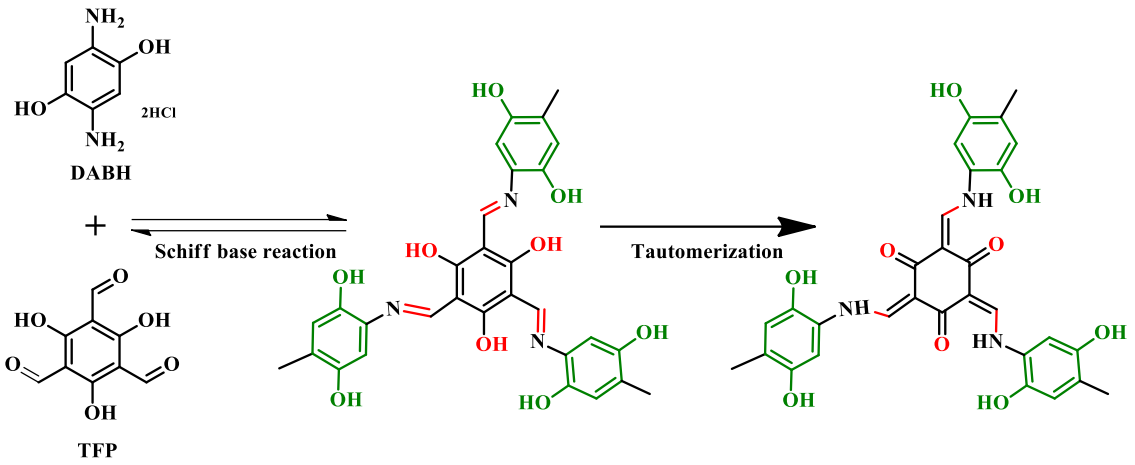

Figure 16: Two-step mechanism of the ß-ketoenamine linkage formation for DABH-TFP-COF. First, a Schiff base reaction yields an imine followed by an enol-keto-tautomerization.

- DABQ-TFP-COF

After DABH-TFP-COF was well characterized, it was reacted with triethylamine under air, to oxidize the hydroquinone linker into the intended linker, benzoquinone.

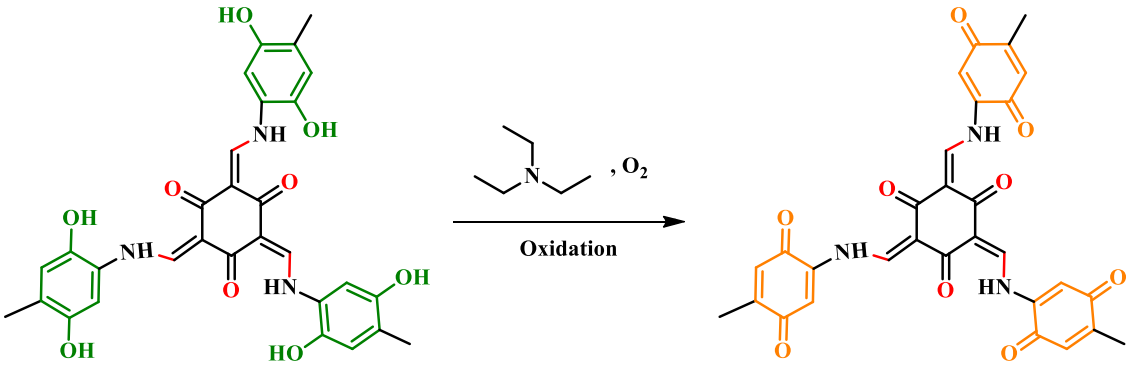

Figure 17: Oxidation reaction of DABH-TFP-COF to DABQ-TFP-COF

The results of the characterization of both DABH-TFP-COF (represented with green color) and DABQ-TFP-COF (represented with orange color) are going to be presented and discussed together, due to the intrinsic connection between the two.

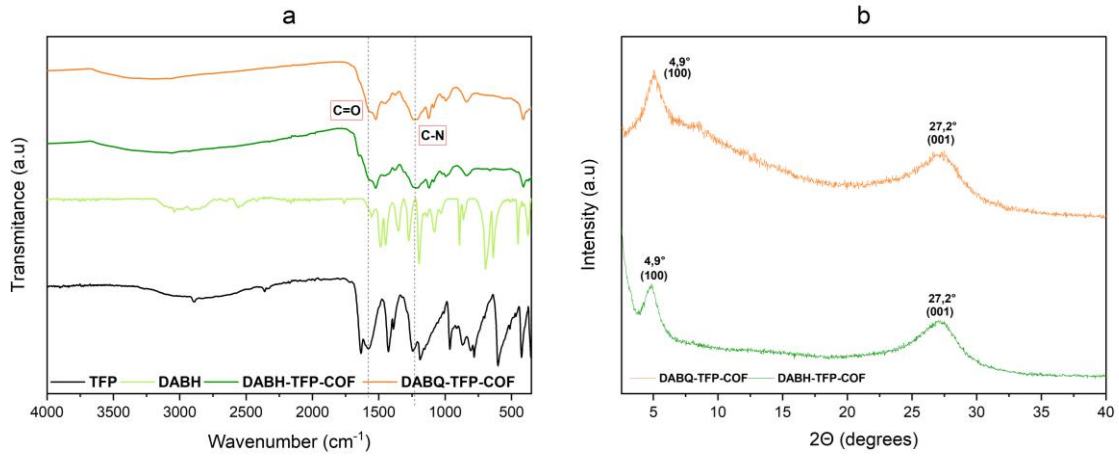

Figure 18: (a) FTIR-ATR spectra related to DABH-TFP-COF and DABQ-TFP-COF as well as the precursors, DABH and TFP. (b) Experimental diffractogram of DABH-TFP-COF and DABQ-TFP-COF.

Analyzing the spectrum obtained from the FTIR-ATR analysis, the band visible at 1250 cm^{-1} for the DABH-TFP-COF indicates the formation of the C-N linkage characteristic of the *β*-ketoenamine framework. Additionally, it is also possible to see a new band formed around 1580 cm^{-1} associated with the C=O bond, also characteristic of a *β*-ketoenamine framework, specifically of the enol-keto tautomerization step.

Both bands are still visible once the COF is oxidized to DABQ-TFP-COF, indicating that the COF's framework remains stable after oxidation. However, it is difficult to conclude by IR if the oxidation of the hydroquinone moieties to benzoquinone was successful.

Next, the diffractogram of DABH-TFP-COF was analyzed, displaying a peak at 4,9° corresponding to the (100) lattice dimension that correlates to the pore diameter of the material, calculated as 1,80 nm. The other visible peak at 27,2° is related to the (001) lattice plan, corresponding to the stacking distance between the 2D COF layers, calculated as 0,33 nm or 33, Å. The peaks found are comparable with the peaks reported in the literature for this COF's framework.[45] Furthermore, the diffractogram obtained for the DABQ-TFP-COF displays the two main peaks in the same location as DABH-TFP-COF, which is expectable since both COFs are expected to present the same lattice structure around the XY plane and along the Z direction.

Next, both COFs were studied by thermal gravimetric analysis, without being previously heated, so an initial weight loss was expected due to the removal of impurities such as solvents, as previously explained. It seems that not accounting for that initial decrease, DABQ-TFP-COF is thermally stable until approximately 300°C. On the other hand, DABH-TFP-COF does not maintain the same degree of stability with temperature. Additionally, both COFs, were just

partially degraded once the test ended at 600°C, DABH-TFP-COF having lost 53% of its weight and DABQ-TFP-COF 57%.

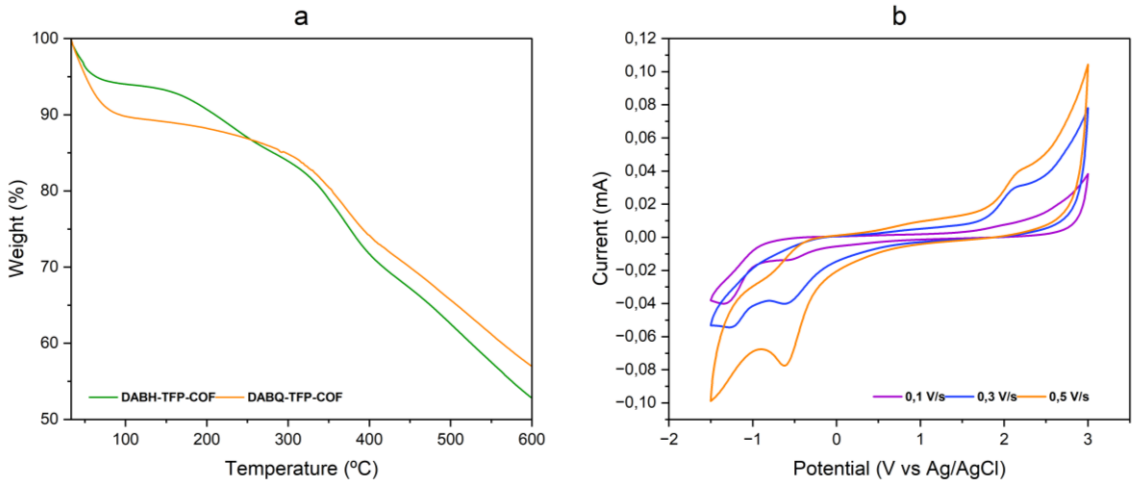

Figure 19: (a) Thermogravimetric analysis (TGA) of DABH-TFP-COF and DABQ-TFP-COF. (b) Cyclic voltammetry of DABQ-TFP-COF at different scan rates.

Lastly, a cyclic voltammetry analysis was done for DABQ-TFP-COF, to analyze the redox processes involved. Three tests were done at three different scan rates, ranging from 0,1 V/s to 0,3 V/s. In the voltammogram, it is possible to see two reversible redox-couple peaks, compatible with the two-electron reversible reduction of benzoquinone to hydroquinone (Figure 7, Chapter 3). The first redox couple has an oxidation peak at around $2{,}15\ V$ and a reduction peak at around $-0{,}61\ V$. The second, redox couple has an oxidation peak at around $-0{,}95\ V$ and a reduction peak at around $-1{,}49V$.

Considering all the characterization techniques used, it is still challenging to claim that DABH-TFP-COF was successfully oxidized to DABQ-TFP-COF. There are some slight differences in the results, but further testing should be conducted to allow for better conclusions.

Nevertheless, taking into consideration the added theoretical capacity and the defined redox processes, it should still be considered the usage of these COFs for electrode material applications.

5.1.3. TTF-DABQ-COF

The synthesis of TTF-DABQ-COF differs from the other two since it has never been reported before. The goal of the design of this reaction is to combine a compound with high capacity, DABQ, with another with higher intrinsic electronic conductivity, a TTF-derived compound with four benzaldehyde groups attached to it, designated as TTF-Ph-TA.

The first parameter that was optimized to try to find a crystalline material was the solvent ratios in the reaction. Four different pairs of solvents were used, namely DMAc/Mesitylene,

Butanol/orto-Dichlorobenzene, and DMAc/1,2,4-Trimethylbenzene. However, none of these solvent combinations yielded crystalline materials. From those, only one showed the characteristic imine linkage band around the interval of 1640 cm^{-1} to 1690 cm^{-1} in the FTIR-ATR spectrum, namely the reaction using DMAc/Mesitylene as solvents. The detailed conditions used and the infrared spectra can be consulted in Appendix A.2

The next possible steps would be to try to optimize the other possible parameters, such as the temperature, reaction time, and catalyst. Alternatively, another synthesis type, such as microwave-assisted synthesis could be tested, since some literature reports are showing promising results employing this technique for the synthesis of imine COFs.[42]

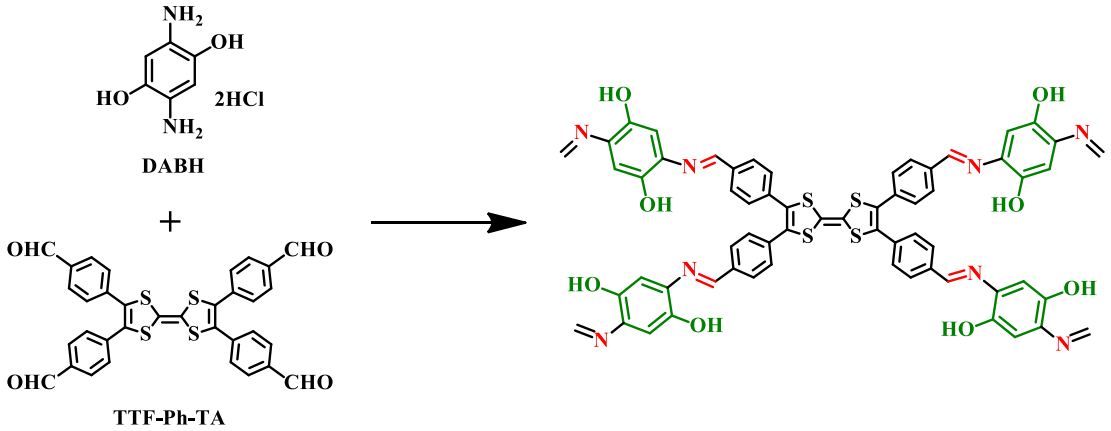

Figure 20: Schematic representation of the TTF-DABH-TFP-COF synthesis.

5.2.Electrochemical Half Cells

Following the detailed characterization of the DAAQ-TFP-COF, the material was used as a positive electrode and was tested using half-cells with lithium metal as the counter and reference electrode. This method is a typical procedure to test new materials for electrodes.

5.2.1. Electrode Preparation and half-cell assembly

Even though no characterization techniques were used, until now, to evaluate the electrode deposition on the current collector, there are still some insights that can be taken from the process.

One important parameter to consider in this step of the process and whose optimization is important is the electrode loading, defined as the quantitative of active material per unit area of the current collector. The average loading obtained was $1{,}27 \pm 0{,}19\, mg/cm^2$. Better control over the loading value is important because using too much or too little active material will have an impact on the performance of the cell. The relation between this parameter and the performance is that a loading value too small, will decrease the capacity of the cell and consequently the energy density. On the other hand, a loading value too high increases significantly the resistance limiting

the electrical current passing the electrode and consequently reducing the cell's rate capability. Nevertheless, our data showed that between the loading values used in our tests, with the range between $0{,}68\ mg/cm^2$ and $1{,}99\ mg/cm^2$, the half-cells that performed better had slightly higher loading values. The detailed measurements and calculations associated with the cell assembly process can be consulted in the Appendix A.5.

Still associated with the loading of the electrode, it is important to optimize the deposition process to obtain the most uniform coating of the slurry possible. Due to trial and error optimization, it was possible to conclude that for our COFs it is crucial to use at least a mortar and pestle to better mix the powdered composite materials. Without this step, the electrode deposition is not as uniform and has the added problem that particles too big tend to not adhere well to the electrode surface, leading to a lot of fall-out particles furthering the problem of irregular coating. This particle fallout was especially perceptible when punching the foil to cut the electrodes but was still noticeable during cell assembly.

5.2.2. Half-cell testing

In total, 15 half-cells were assembled following the same procedure, the only difference being the slight optimization of the cathode preparation in the last four cells. However, not all those cells were studied and tested to the same extent and in this section, the comparison of the results of 7 of those cells will be discussed.

Once the half-cells were properly assembled, they were immediately tested with a multimeter to obtain the open-circuit voltage. The voltages tended to rage between 1,5V and 3V. In Table 3 the OCV obtained as soon as the assembly was finished is represented as well as the OCV measure in other situations for some of those cells.

Table 3: Summary of the OCV values obtained once the cell was assembled inside the glovebox and the lowest and highest values of other OCV measured after that. Cell A and B were just measured once.

Cell	First OCV (V)	Lowest OCV (V)	Highest OCV (V)
A	2,57	-	-
B	2,515	-	-
C	2,355	1,101	2,355
D	1,942	1,942	2,385
E	3,106	3,007	3,604
F	2,112	2,112	2,770

The open-circuit voltage measured for these cells is around the values expected for the type of coin-cell assembled used, with lithium metal as the reference electrode and aluminum as the positive electrode current collector. [46]

5.2.2.1. Potentiostatic Electrochemical Impedance Spectroscopy (PEIS)

The first electrochemical test done to the electrochemical cells, once they were left to rest for a few hours at least, is the potentiostatic electrochemical impedance spectroscopy. The cell response was first plotted in a Nyquist plot. The type of plot obtained differed among cells, but most had a plot behavior relatively similar to the one illustrated in Figure 21 for cell A.

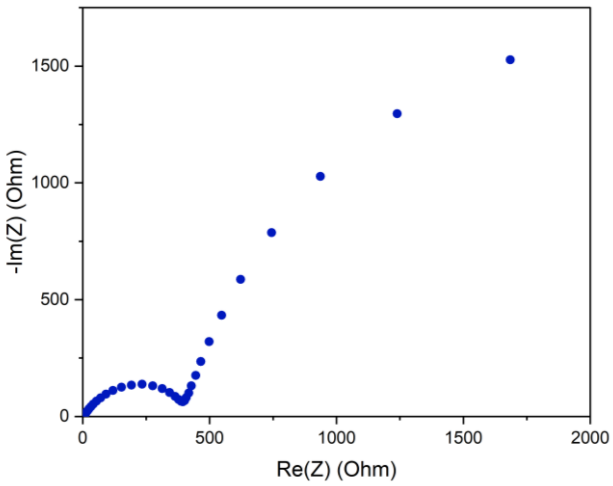

Figure 21: Nyquist plot for cell A obtained through PEIS

Then, the goal was to determine the resistances associated with the higher and middle frequencies, the semi-circle represented in the Nyquist plot. To do this, the data were fitted using the EC-Lab z-fit software, to the electric circuit represented in Figure 22.

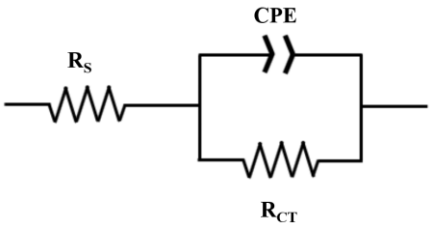

Figure 22. Equivalent circuit associated with the Nyquist plots obtained.

In the equivalent circuit used, R_s represents the solution resistance; R_{ct} corresponds to the charge transfer resistance and CPE symbolizes the constant phase element. It is the CPE that takes into account the pseudocapacitance associated with the solid electrolyte interphase, the layer formed between the electrolyte and the electrode. The values obtained for each parameter for each cell are summarized in Table 4.

Table 4: Summary of the solution resistance (R_S), the charge transfer resistance (R_{CT}) and the constant phase element (CPE) for all the cells.

Cell	R_S (Ohm)	R_{CT} (Ohm)	CPE (F)
A	3,353	416,4	$6{,}90 \times 10^{-06}$
B	4,624	120,0	$0{,}66 \times 10^{-06}$
C	4,503	345,9	$1{,}06 \times 10^{-06}$
D	3,283	622,8	$3{,}99 \times 10^{-06}$
E	4,100	649,7	$2{,}48 \times 10^{-06}$
F	2,704	162,2	$2{,}53 \times 10^{-06}$

Still using the data provided by the PEIS analysis, in this case, the frequency, it is possible to obtain the Warburg coefficient, σ, using Equation 11 (Chapter 4). In this case, just the data associated with the lowest frequency is plotted since the Warburg coefficient is associated with those values. The Warburg coefficient corresponds to the slope of the tendency line fitted to the data, as represented in Figure 23 for cell A.

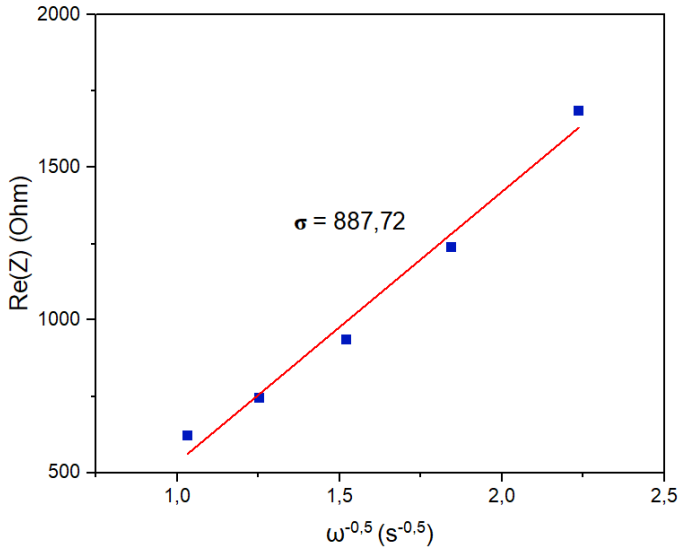

Figure 23: Plot to determine the Warburg coefficient, through the slope of the fitted data.

The value used as an example is the biggest value obtained from all the cells, and it was possible to infer that the value was going to be high just by analyzing the Nyquist plot. The area more to the right of a Nyquist plot is associated with lower frequencies and subsequently slower processes such as diffusion and specific the Warburg diffusion. Next, using the values obtained for the Warburg diffusion it was possible to calculate the lithium-ion diffusion coefficient (D_{Li^+}) using Equation 8 (Chapter 4). The results are summarized in Table 5.

Table 5: Summary of the values obtained for the Warburg and the lithium-ion diffusion coefficients, for all the cells.

Cell	σ (-)	D_{Li^+} (cm^2/s)
A	887,72	$1{,}71 \times 10^{-13}$
B	11,093	$1{,}30 \times 10^{-09}$
C	156,38	$5{,}80 \times 10^{-10}$
D	237,47	$1{,}32 \times 10^{-11}$
E	42,978	$5{,}20 \times 10^{-11}$
F	22,570	$3{,}28 \times 10^{-10}$

The Warburg coefficient and the lithium-ion diffusion coefficient are inversely proportional, since the greatest the Warburg impedance element value, the highest resistance to the flow of ions, and consequently slower ion diffusion of those ions. The reported values[12] for the lithium-ion coefficients of inorganic electrode oscillate between $5{,}2 \times 10^{-14}$ to $1{,}7 \times 10^{-11}$ cm^2/s, meaning cells diffusion of the lithium-ion in the electrode that is up to commercial standards, with even slightly better values.

Taking into account that our active material, the DAAQ-TFP-COF is a highly crystalline porous material, the enhance lithium-ion diffusion on the pores can be correlated with the COF structure since the pores work as channels for facilitated ion diffusion.

5.2.2.2. Cyclic Voltammetry (CV)

Since the electrochemical processes of the cell are governed by the oxidation and reduction reactions that occur in the electrodes it is crucial to study those redox reactions by cyclic voltammetry.

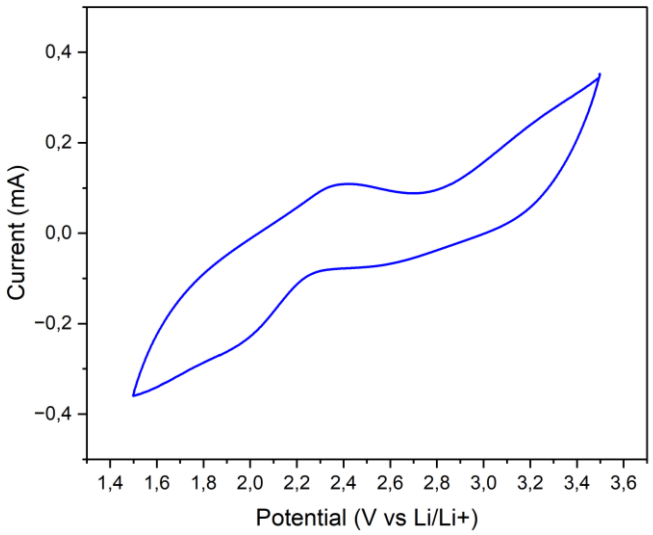

Figure 24: Cyclic voltammogram of cell D using DAAQ-TFP-COF as the positive electrode.

Through the voltammogram in Figure 24, it is visible that at least one oxidation and one reduction peaks at around 2,4 V and 1,99 V respectively.

5.2.2.3. Cycling performance Tests

After all the cells were well characterized, they were subjected to charge and discharge cycles to access their electrochemical performance. Since the DAAQ-TFP-COF used as the active material for the positive electrode is not lithiated, it is important to start the cycling tests with discharge, to allow a flow of lithium ions to access the positive electrode and lithiated it.

These tests were performed differently in two different groups of cells. In one group, the cells were subjected just to the constant current during all the charge and discharge cycles. In the second group, a constant voltage charge cycle was also introduced.

- Constant Current

Using this type of charge and discharge, the cells were always subjected to the same current. The charge-discharge curves for the first and second cycles for cell B, are represented in Figure 25 and the cycling performance during 60 cycles, is represented in Figure 26.

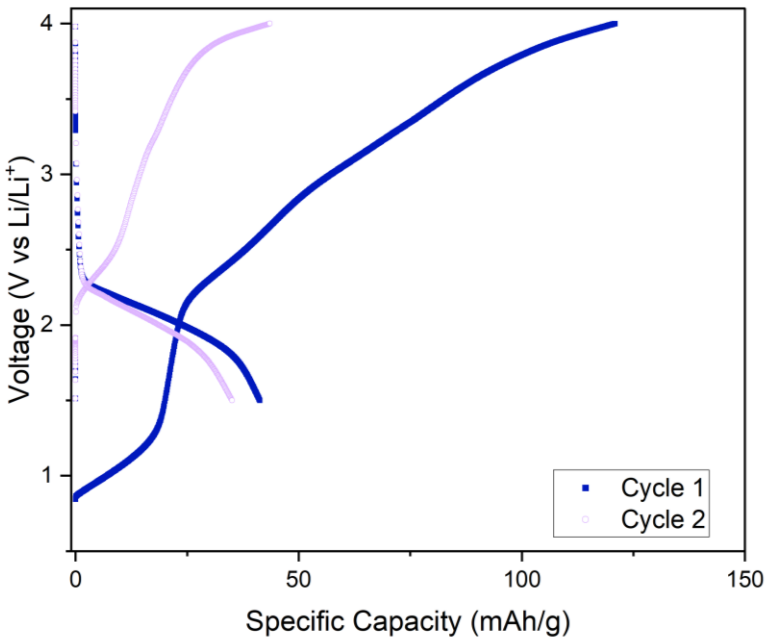

Figure 25: Charge-Discharge curves of cell B at cycles 1 and 2.

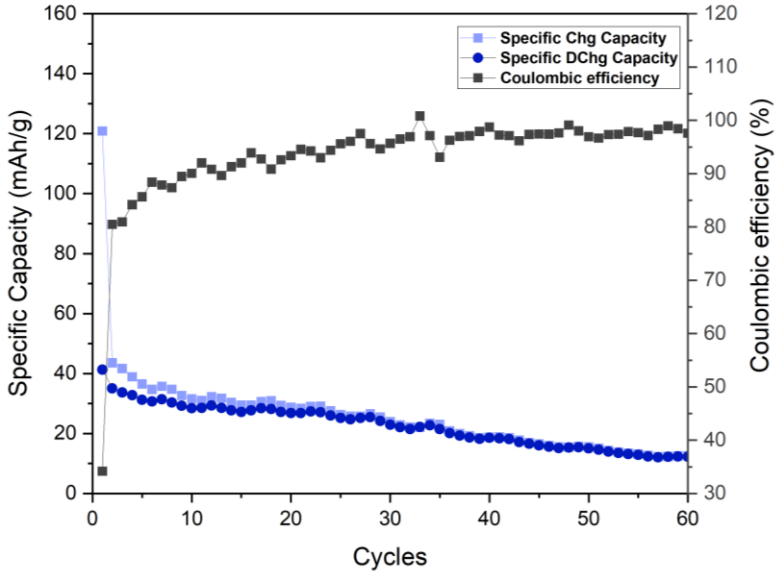

Figure 26: Cycling performance of cell B, of discharge and charge, until cycle number 60 and the respective Coulombic Efficiency.

Analyzing both graphs, it is possible to notice a big specific capacity drop after the first cycle, the charge-specific capacity went from 120 mAh/g, the highest value of all the cells, to just 43,57 mAh/g in the second cycle. On the other hand, the discharge-specific capacity also suffers a drop albeit much smaller, from 41,29 mAh/g to 35,06 mAh/g.

Several reasons can cause this kind of drop in capacity from the first to the second cycle. One of the possible reasons is related to the formation of the solid electrolyte interphase. This type of capacity loss is irreversible and should be reduced. However, it is also crucial to remember the role the SEI has in maintaining electrochemical stability.

Another possible reason could be related to the relatively easy desegregation of the material from the electrode current collector. Active material that is not placed in the electrode could not just decrease the specific capacity directly, but it could also be related to the unwanted reaction inside the cell.

Finally, the irregular and bulky constitution of the DAAQ-TFP-COF can also be a reason for the capacity loss. Even though bulk COFs do have a porous structure that can create perfectly aligned channels, most of the time these pores are not aligned, and the lithium-ion diffusion after the first cycle becomes sluggish due to this reason.

Nevertheless, the material shows promising behavior and with further optimization of the process could yield even better results. To further optimize the process, it is also important to better understand the behavior of the DAAQ-TFP-COF as an electrode material, with that, the planned

soft X-ray Transmission Microscopy analyses will be crucial to better study the reversible redox reactions and lithiation processes.

- Constant Current + Constant Voltage

During these tests, a constant voltage charge followed the constant current charge of the cell. The constant charge allows the charge of the cell once the maximum voltage is reached the charge switches to constant voltage. This type of charge cycle is often used within the cell manufacturing industry since it allows for a more stable charge cycle and increases the cycle life of the cell, since it prevents the occurrence of some irreversible reactions that are associated with a drop in the capacity. The resulting cycling performance assessments are relatively different and the specific capacity doesn't have an exponential drop from the first cycle. Figure 27 illustrates the behavior of cell E.

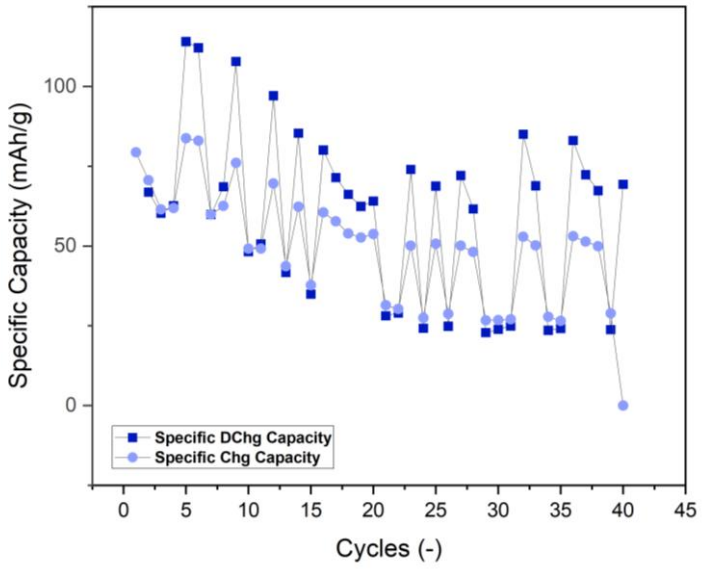

Figure 27: Charge and discharge cycling performance of cell E.

Here, the maximum achieved specific capacity is not the one of the first cycle and there is clear better stability of that capacity along with the cycles.

Finally, when looking at all the parameters determined (Appendix A.5and A.7), from the open-circuit voltage to the resistances and the lithium-ion coefficient obtained through PEIS, there is a clear relationship between the optimization of those parameters and the better cycling performance of the cell. The cells that had better results, B, E, and F are the ones associated with relatively higher OCVs and relatively lower resistance elements. As well as being the ones that have the smallest Warburg coefficients and the highest lithium-ion coefficient values, further highlighting the big influence that ionic and electronic transport has on the cells' performance.

6. Conclusion and future work

At beginning of this dissertation, the goals were focused on exploring the role of covalent organic framework materials as electrodes for lithium-ion batteries.

Even though the synthesis of a new covalent organic framework with optimized properties for the use as electrode materials was not achieved, for now, the steps in the right direction have been taken.

Additionally, the detailed study of DAAQ-TFP-COF as a positive electrode, have allowed a better understanding of all the processes involved from designing a new material to its final application. This detailed characterization from the material to the use in an electrochemical cell was crucial to the proper understanding of the procedures, techniques, and methodologies.

The results are indeed promising and open the door for many more exploration opportunities. One of those exploration paths is the one that focuses on understanding even better the chemistry and physics that govern these materials and the intrinsic relation between the material and the performance of the battery. New characterization techniques, such as the Soft X-ray Transmission Microscopy analyses, that are already planned for the near future are crucial.

As the discussion of this work and the literature suggests, the exfoliation of COFs should yield even better performance results and the steps were already taken to start studying different exfoliation methods and the effect they have on the COFs' performance as an electrode material.

Furthermore, the design of new COF materials should be kept being explored. The process is not always straightforward and can involve a lot of trial-and-error iterations, but it is crucial to keep extending the boundaries of COFs as useful electroactive materials.

Moreover, the exploration of COFs with solid electrolytes instead of the usual liquid electrolyte should be explored, since those are the electrolytes that will make up the future of the battery world, due to their increased safety and other additional benefits.

Lastly, the studying of COFs as electrodes should be expanded further to other battery technologies, especially the ones that further explore the search for a more sustainable energy storage solution.

7. References

[1] Independent Evaluation Office (IEO) of the United Nations Development Programme (UNDP), Evaluation of UNDP Support to Energy Access and Transition, 2021.

[2] International Energy Agency, Renewables 2021 - Analysis and forecast to 2026, 2021. www.iea.org/t&c/.

[3] European Commission, Energy storage - the role of electricity, 2017.

[4] European Commission, Study on energy storage-Contribution to the security of the electricity supply in Europe, 2020. https://doi.org/10.2833/077257.

[5] T. Sun, J. Xie, W. Guo, D.S. Li, Q. Zhang, Covalent–Organic Frameworks: Advanced Organic Electrode Materials for Rechargeable Batteries, Advanced Energy Materials. 10 (2020). https://doi.org/10.1002/aenm.201904199.

[6] É. Lèbre, M. Stringer, K. Svobodova, J.R. Owen, D. Kemp, C. Côte, A. Arratia-Solar, R.K. Valenta, The social and environmental complexities of extracting energy transition metals, Nature Communications. 11 (2020). https://doi.org/10.1038/s41467-020-18661-9.

[7] M. Armand, J.-M. Tarascon, Building better batteries, Nature. (2008). https://doi.org/10.1038/451652a.

[8] Y. Lu, J. Chen, Prospects of organic electrode materials for practical lithium batteries, Nature Reviews Chemistry. 4 (2020) 127–142. https://doi.org/10.1038/s41570-020-0160-9.

[9] Y. Lu, Q. Zhang, L. Li, Z. Niu, J. Chen, Design Strategies toward Enhancing the Performance of Organic Electrode Materials in Metal-Ion Batteries, Chem. 4 (2018) 2786–2813. https://doi.org/10.1016/j.chempr.2018.09.005.

[10] T.B. Reddy, Linden's Handbook Of Batteries, 4th ed., McGraw-Hill, 2011.

[11] C. Julien, A. Mauger, A. Vijh, K. Zaghib, Lithium Batteries: Science and Technology, Springer, 2016.

[12] S. Wang, Q. Wang, P. Shao, Y. Han, X. Gao, L. Ma, S. Yuan, X. Ma, J. Zhou, X. Feng, B. Wang, Exfoliation of Covalent Organic Frameworks into Few-Layer Redox-Active Nanosheets as Cathode Materials for Lithium-Ion Batteries, J Am Chem Soc. 139 (2017) 4258–4261. https://doi.org/10.1021/jacs.7b02648.

[13] E. Vitaku, C.N. Gannett, K.L. Carpenter, L. Shen, H.D. Abruña, W.R. Dichtel, Phenazine-Based Covalent Organic Framework Cathode Materials with High Energy and Power Densities, J Am Chem Soc. 142 (2019) 16–20. https://doi.org/10.1021/jacs.9b08147.

[14] R. Tian, S.-H. Park, P.J. King, G. Cunningham, J. Coelho, V. Nicolosi, J.N. Coleman, Quantifying the factors limiting rate-performance in battery electrodes, n.d.

[15] S. Wang, Y. Fan, D.-I. Stroe, C. Fernandez, C. Yu, W. Cao, Z. Chen, Battery state estimation methods, Battery System Modeling. (2021) 125–156. https://doi.org/10.1016/B978-0-323-90472-8.00001-9.

[16] J.B. Goodenough, K.S. Park, The Li-ion rechargeable battery: A perspective, J Am Chem Soc. 135 (2013) 1167–1176. https://doi.org/10.1021/ja3091438.

[17] A. Wang, S. Kadam, H. Li, S. Shi, Y. Qi, Review on modeling of the anode solid electrolyte interphase (SEI) for lithium-ion batteries, Npj Computational Materials. 4 (2018). https://doi.org/10.1038/s41524-018-0064-0.

[18] J. Xie, Y.C. Lu, A retrospective on lithium-ion batteries, Nature Communications. 11 (2020). https://doi.org/10.1038/s41467-020-16259-9.

[19] The Royal Swedish Academy of Sciences, Scientific Background on the Nobel Prize in Chemistry 2019: Lithium-ion Batteries, 2019.

[20] A. Manthiram, A reflection on lithium-ion battery cathode chemistry, Nature Communications 2020 11:1. 11 (2020) 1–9. https://doi.org/10.1038/s41467-020-15355-0.

[21] R.C. Massé, C. Liu, Y. Li, L. Mai, G. Cao, Energy storage through intercalation reactions: Electrodes for rechargeable batteries, National Science Review. 4 (2017) 26–53. https://doi.org/10.1093/nsr/nww093.

[22] P. Poizot, J. Gaubicher, S. Renault, L. Dubois, Y. Liang, Y. Yao, Opportunities and Challenges for Organic Electrodes in Electrochemical Energy Storage, Chemical Reviews. 120 (2020) 6490–6557. https://doi.org/10.1021/acs.chemrev.9b00482.

[23] A.P. Côte, A.I. Benin, N.W. Ockwig, M. O'Keeffe, A.J. Matzger, O.M. Yaghi, Porous, Crystalline, Covalent Organic Frameworks, Science (1979). 310 (2005) 1166–1170. https://doi.org/DOI: 10.1126/science.1120411.

[24] K. Geng, T. He, R. Liu, S. Dalapati, K.T. Tan, Z. Li, S. Tao, Y. Gong, Q. Jiang, D. Jiang, Covalent Organic Frameworks: Design, Synthesis, and Functions, Chemical Reviews. 120 (2020) 8814–8933. https://doi.org/10.1021/acs.chemrev.9b00550.

[25] C.S. Diercks, O.M. Yaghi, The atom, the molecule, and the covalent organic framework, Science (1979). 355 (2017). https://doi.org/10.1126/science.aal1585.

[26] F. Haase, B. v. Lotsch, Solving the COF trilemma: Towards crystalline, stable and functional covalent organic frameworks, Chemical Society Reviews. 49 (2020) 8469–8500. https://doi.org/10.1039/d0cs01027h.

[27] M.S. Lohse, T. Bein, Covalent Organic Frameworks: Structures, Synthesis, and Applications, Advanced Functional Materials. 28 (2018). https://doi.org/10.1002/adfm.201705553.

[28] J. Li, X. Jing, Q. Li, S. Li, X. Gao, X. Feng, B. Wang, Bulk COFs and COF nanosheets for electrochemical energy storage and conversion, Chemical Society Reviews. 49 (2020) 3565–3604. https://doi.org/10.1039/d0cs00017e.

[29] M. Souto, D.F. Perepichka, Electrically conductive covalent organic frameworks: Bridging the fields of organic metals and 2D materials, Journal of Materials Chemistry C. 9 (2021) 10668–10676. https://doi.org/10.1039/d1tc00750e.

[30] S. Kandambeth, A. Mallick, B. Lukose, M. v. Mane, T. Heine, R. Banerjee, Construction of crystalline 2D covalent organic frameworks with remarkable chemical (Acid/Base) stability via a combined reversible and irreversible route, J Am Chem Soc. 134 (2012) 19524–19527. https://doi.org/10.1021/ja308278w.

[31] C.R. Deblase, K.E. Silberstein, T.T. Truong, H.D. Abruña, W.R. Dichtel, β-ketoenamine-linked covalent organic frameworks capable of pseudocapacitive energy storage, J Am Chem Soc. 135 (2013) 16821–16824. https://doi.org/10.1021/ja409421d.

[32] P.J. Waller, F. Gándara, O.M. Yaghi, Chemistry of Covalent Organic Frameworks, Accounts of Chemical Research. 48 (2015) 3053–3063. https://doi.org/10.1021/acs.accounts.5b00369.

[33] Y. Lu, Y. Cai, Q. Zhang, J. Chen, Structure-Performance Relationships of Covalent Organic Framework Electrode Materials in Metal-Ion Batteries, Journal of Physical Chemistry Letters. 12 (2021) 8061–8071. https://doi.org/10.1021/acs.jpclett.1c02004.

[34] X. Zhao, P. Pachfule, A. Thomas, Covalent organic frameworks (COFs) for electrochemical applications, Chemical Society Reviews. 50 (2021) 6871–6913. https://doi.org/10.1039/d0cs01569e.

[35] Z. Song, H. Zhan, Y. Zhou, Anthraquinone based polymer as high performance cathode material for rechargeable lithium batteries, Chemical Communications. (2009) 448–450. https://doi.org/10.1039/b814515f.

[36] W. Wang, W. Xu, L. Cosimbescu, D. Choi, L. Li, Z. Yang, Anthraquinone with tailored structure for a nonaqueous metal-organic redox flow batter, Chemical Communications. 48 (2012) 6669–6671. https://doi.org/10.1039/c2cc32466k.

[37] N. Monni, M.S. Angotzi, M. Oggianu, S.A. Sahadevan, M.L. Mercuri, Redox-active benzoquinones as challenging “non-innocent” linkers to construct 2D frameworks and nanostructures with tunable physical properties, Journal of Materials Chemistry C. 10 (2022) 1548–1572. https://doi.org/10.1039/D1TC05335C.

[38] H.W. Lerner, G. Margraf, T. Kretz, O. Schiemann, J.W. Bats, G. Dürner, F.F. de Biani, P. Zanello, M. Bolte, M. Wagner, Redox behaviour of pyrazolyl-substituted 1,4-dihydroxyarenes: Formation of the corresponding semiquinones, quinhydrones and quinones, Zeitschrift Fur Naturforschung - Section B Journal of Chemical Sciences. 61 (2006) 252–264. https://doi.org/10.1515/znb-2006-0304.

[39] M. Souto, K. Strutyński, M. Melle-Franco, J. Rocha, Electroactive Organic Building Blocks for the Chemical Design of Functional Porous Frameworks (MOFs and COFs) in Electronics, Chemistry - A European Journal. 26 (2020) 10912–10935. https://doi.org/10.1002/chem.202001211.

[40] D. Rodríguez-San-Miguel, C. Montoro, F. Zamora, Covalent organic framework nanosheets: Preparation, properties and applications, Chemical Society Reviews. 49 (2020) 2291–2302. https://doi.org/10.1039/c9cs00890j.

[41] T. Li, X. Yan, W. da Zhang, W.K. Han, Y. Liu, Y. Li, H. Zhu, Z. Li, Z.G. Gu, A 2D donor-acceptor covalent organic framework with charge transfer for supercapacitors, Chemical Communications. 56 (2020) 14187–14190. https://doi.org/10.1039/d0cc04109b.

[42] S.L. Cai, Y.B. Zhang, A.B. Pun, B. He, J. Yang, F.M. Toma, I.D. Sharp, O.M. Yaghi, J. Fan, S.R. Zheng, W.G. Zhang, Y. Liu, Tunable electrical conductivity in oriented thin films of tetrathiafulvalene-based covalent organic framework, Chemical Science. 5 (2014) 4693–4700. https://doi.org/10.1039/c4sc02593h.

[43] I.A. Lázaro, A Comprehensive Thermogravimetric Analysis Multifaceted Method for the Exact Determination of the Composition of Multifunctional Metal-Organic Framework

Materials, European Journal of Inorganic Chemistry. 2020 (2020) 4284–4294. https://doi.org/10.1002/ejic.202000656.

[44] N. Elgrishi, K.J. Rountree, B.D. McCarthy, E.S. Rountree, T.T. Eisenhart, J.L. Dempsey, A Practical Beginner's Guide to Cyclic Voltammetry, Journal of Chemical Education. 95 (2018) 197–206. https://doi.org/10.1021/acs.jchemed.7b00361.

[45] A.M. Khayum, M. Ghosh, V. Vijayakumar, A. Halder, M. Nurhuda, S. Kumar, M. Addicoat, S. Kurungot, R. Banerjee, Zinc ion interactions in a two-dimensional covalent organic framework based aqueous zinc ion battery, Chemical Science. 10 (2019) 8889–8894. https://doi.org/10.1039/c9sc03052b.

[46] S. Trasatti, The absolute electrode potential : an explanatory note (Recommendations 1986), 1986.

8. Appendix

A.1. BET Surface Area

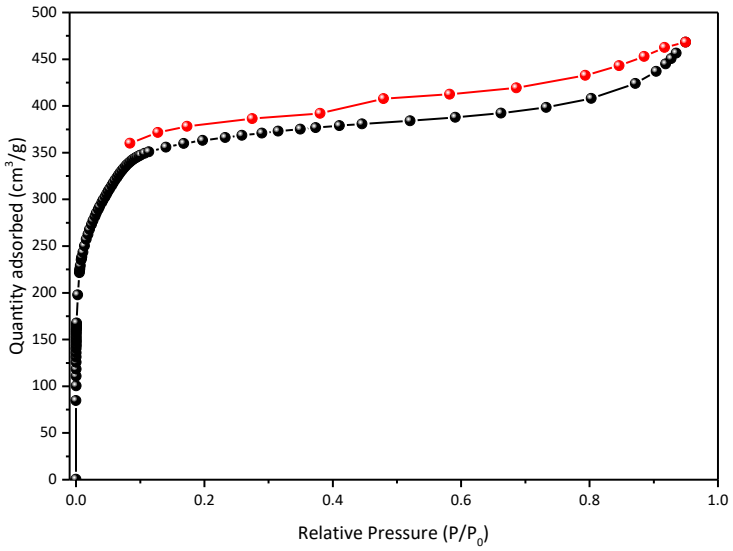

Figure A.1. Nitrogen adsorption isotherm. measured through a collaboration with Prof. Felix Zamora from the Universidad Autónoma de Madrid (UAM).

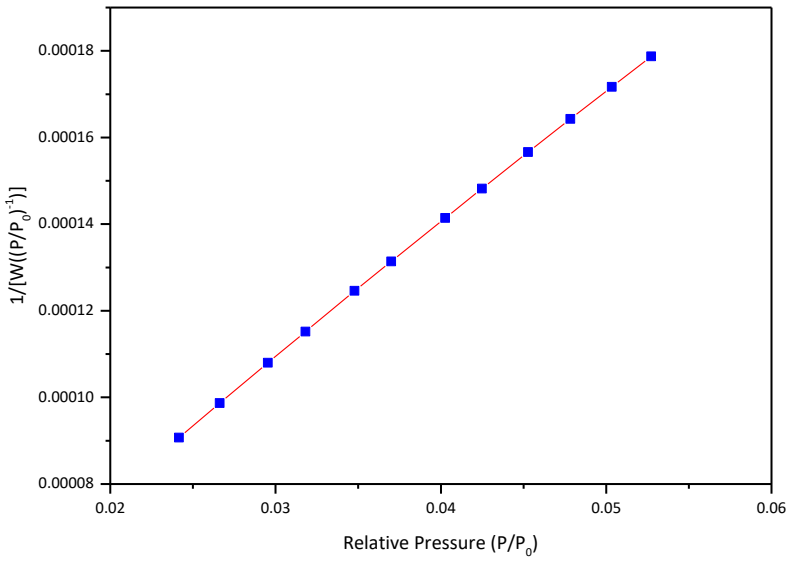

Figure A.2. BET linear fitting, used to obtain the BET surface area.

Parameters obtained:

- BET surface area: 1407 ± 6,483 m²/g
- Slope: 0.06897 ± 0,000319 g/mmol
- Correlation coefficient: 0,9999
- Molecular cross-sectional area: 0,1620 nm²

A.2. SEM and EDS results

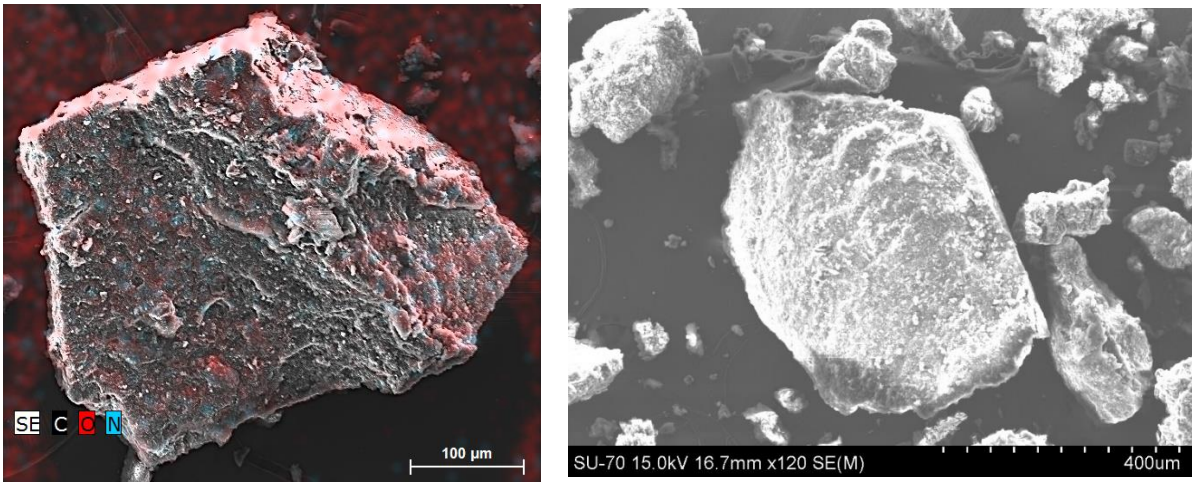

Figure A.3: Scanning electron microscopy (SEM) images of DAAQ-TFP-COF as a bulk powder.

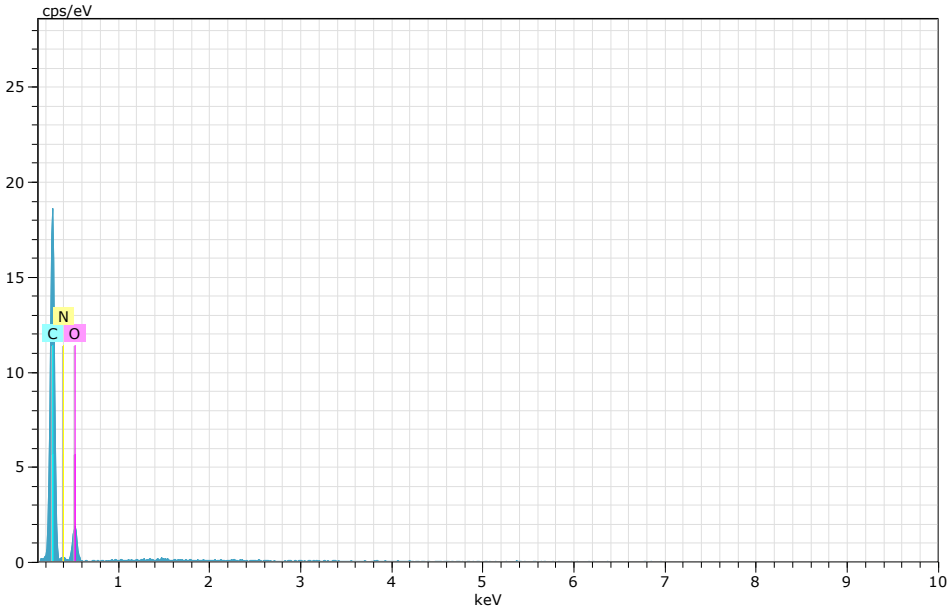

Figure A.4: Graphical representation of the composition of DAAQ-TFP-COF obtained using EDS.

Table A.1: Proportion of elements in DAAQ-TFP-COF represented as weight concentration and atomic weight , as well as the corresponding error. Obtained with EDS.

Element	Series	Unn. C [wt.%]	Norm. C [wt.%]	Atom. C [at.%]	Error (3 Sigma) [wt.%]
Carbon	K-series	69.89	69.89	74.82	27.96
Oxygen	K-series	21.52	21.52	17.29	12.95
Nitrogen	K-series	8.59	8.59	7.89	9.29
Total		100.00	100.00	100.00	

- **Unn. C [wt.%]:** unnormalized concentration in weight percent of the element.
- **Norm. C [wt.%]:** normalised concentration in weight percent of the element.
- **Atom. C [at.%]:** atomic weight percent.
- **Error (3 Sigma) [wt.%]:** error in the weight percent concentration.

A.3. Synthesis of TTF-DABH-COF

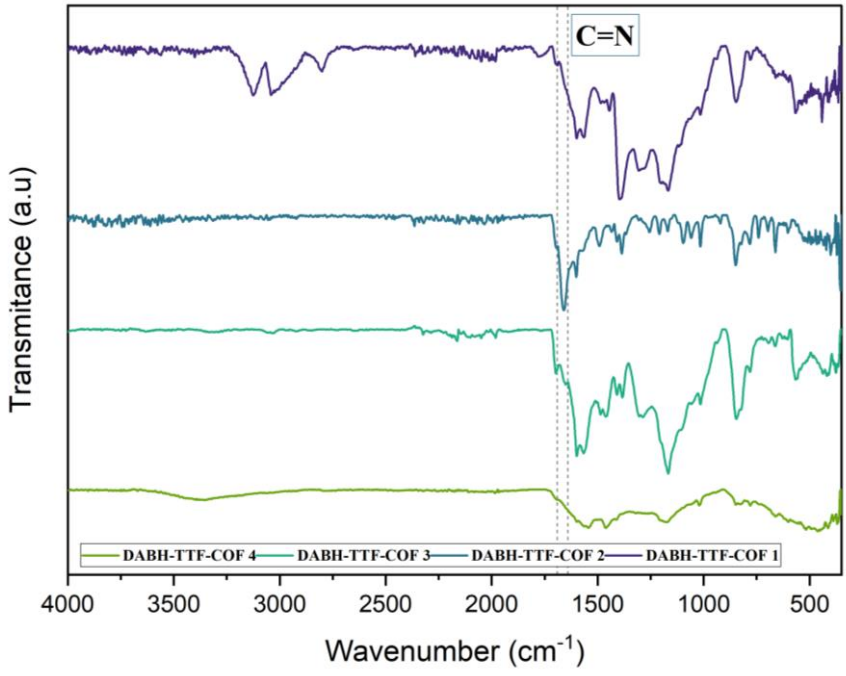

Figure A.5: FTIR-ATR spectra related to the different assays of the TTF-DABH-COF synthesis. The dashed lines denote the region of the imine linkage (1640-1690 cm^{-1}).

Table A.2. Parameters used for the different assays of TTF-DABH-COF synthesis.

Assay	Precursors				Solvents				Modulator		Oven Conditions		Yield Calculations		
	TTF-Ph-TA (mg)	TTF-Ph-TA (mmol)	DABH (mg)	DABH (mmol)	Solvent 1	Volume 1 (mL)	Solvent 2	Volume 2 (mL)	Name	Volume (mL)	T (°C)	Days	COF Theoretical Mass (mg)	COF Mass (mg)	Yield (%)
1	13,6	0,0219	9,6	0,0451	Dioxane	0,5	Mesitylene	0,5	AcOH 3M	0,1	120	3	15,28	8,6	56,33
2	10	0,0161	5	0,0235	DMAc	0,5	Mesitylene	0,5	AcOH 6M	0,05	120	3	11,23	12,8	114,02
3	20	0,0322	10	0,0469	Butanol	0,1	oDCB	1,9	AcOH 6M	0,2	130	3	22,45	5,1	22,71
4	14,6	0,0235	10	0,0469	1,2,4-Trimethylbenzol	1,75	DMAc	0,25	AcOH 3M	0,2	120	3	16,39	9,2	56,13

A.4. Slurry and electrode preparation

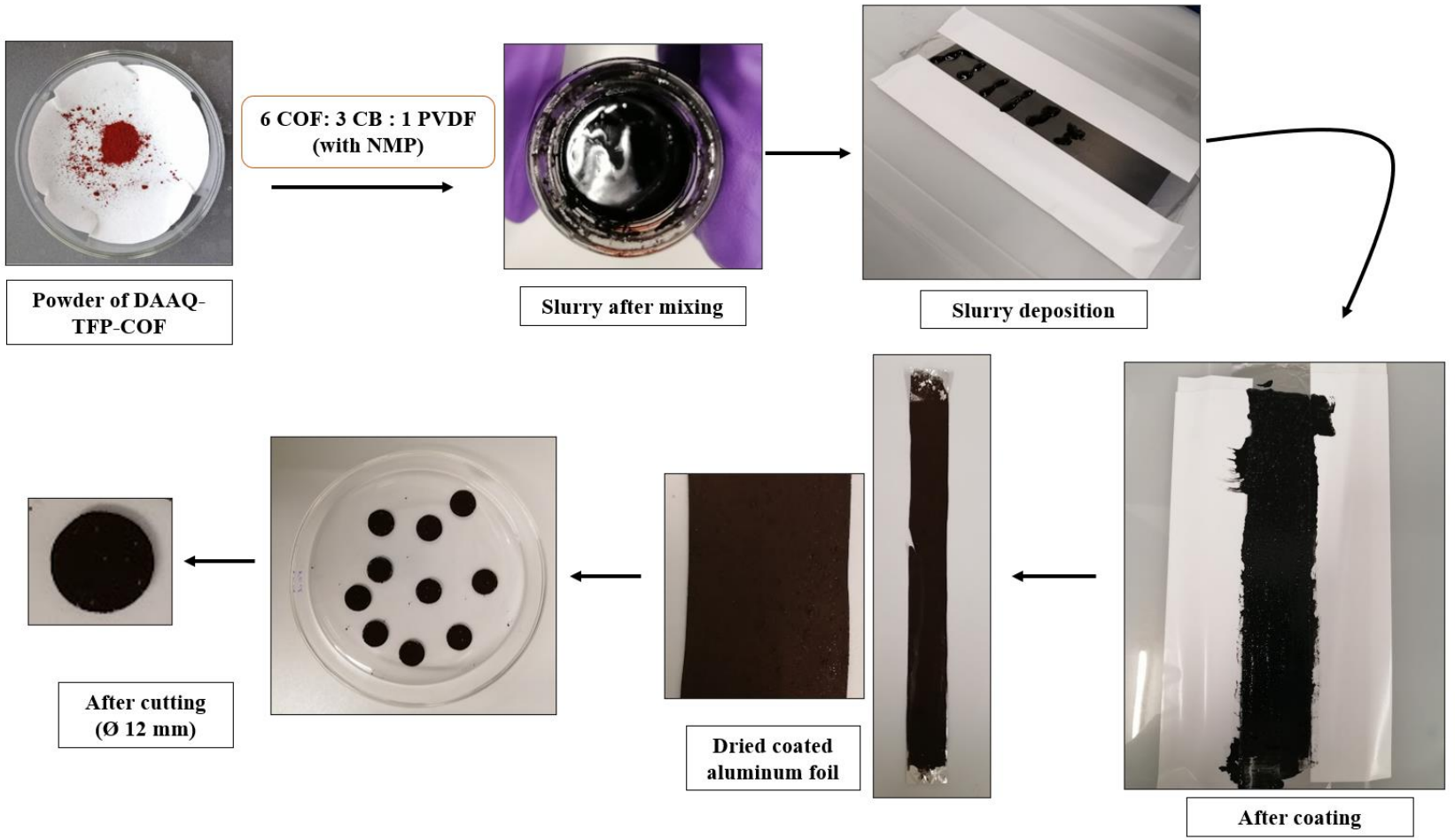

Figure A.6: Schematic representation of the slurry and electrode preparation, using pictures taken during the laboratory process.

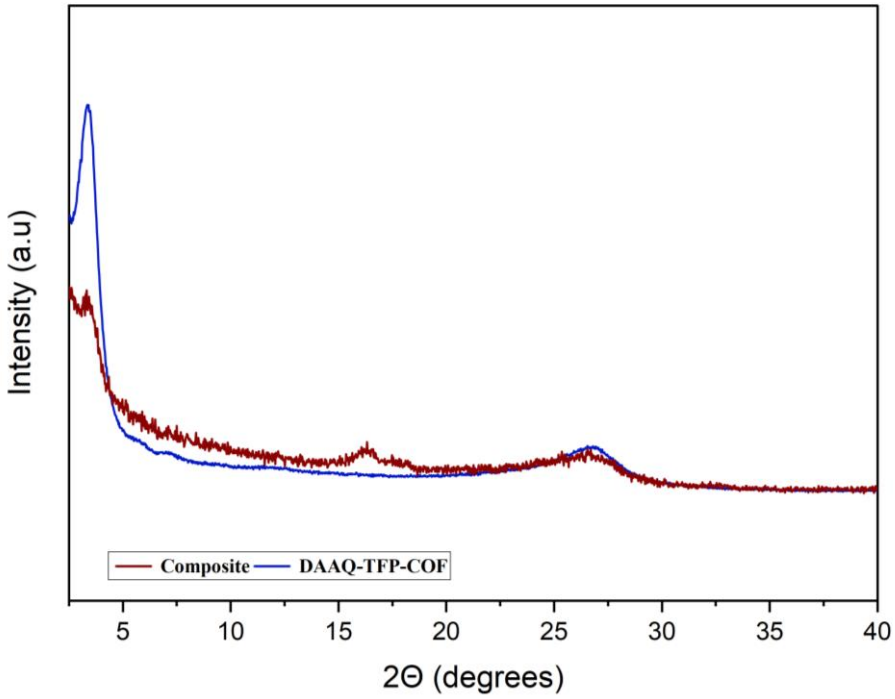

Figure A.7. Diffractogram of DAAQ-TFP-COF and the electrode composite (DAAQ-TFP-COF, carbon black and PVDF). The composite used was obtained through the disintegration of a prepared electrode.

A.5. Coin-cell assembly

Table A.3: Summary of the weighted lithium metal and cathode material for each cell initially assembled and tested.

Group	Cell nº per group	Cell	Lithium Weight (mg)	Total Cathode Weight (mg)	Cathode coating weight (mg)	COF per cathode (mg)	COF loading (mg/cm^2)
1	**1**	-	30,9	7,7	2,7	1,59	1,41
	2	-	37,5	6,8	1,8	1,05	0,93
	3	-	38,9	7,5	2,5	1,47	1,30
	4	-	32,9	7,2	2,2	1,29	1,14
	5	**A**	28,7	8,4	3,4	2,01	1,78
	6	**B**	29,8	8,8	3,8	2,25	1,99
	7	-	31,5	8,0	3,0	1,77	1,57
2	**5**	**C**	37,0	7,2	2,1	1,27	1,12
	6	**D**	24,9	6,3	1,3	0,77	0,68
	7	**E**	26,4	6,8	1,7	1,03	0,91
	8	**F**	38,5	7,1	2,1	1,25	1,11

The loading of each electrode was calculated using Equation A.1, where m_{COF} represents the weight of the COF loaded onto the electrode and D represents the diameter of the electrode, in this case 12 mm. The average loading was calculated using Equation A.2. Next, using Equation A.3, the uncertainty associated with the loading was determined using the uncertainties of the instruments used for the measurements, in this case the uncertainty of the laboratory scale weighting (Δm_{COF}) and the electrode cutter (ΔD). The results are represented in Table A.4.

$$Loading\ of\ electrode\ i\ (L_i) = \frac{m_{COF}}{Area} = \frac{m_{COF}}{\pi \cdot \left(\frac{D}{2}\right)^2} \tag{A.1}$$

$$\bar{L} = \frac{\sum L_i}{N} \tag{A.2}$$

$$\Delta L = \left|\frac{\partial L}{\partial m_{COF}}\right| \cdot \Delta m_{COF} + \left|\frac{\partial L}{\partial D}\right| \cdot \Delta D = \frac{4}{\pi \cdot D^2} \cdot \Delta m + \frac{8 \cdot \overline{m_{COF}}}{\pi \cdot D^3} \cdot \Delta D \tag{A.3}$$

Table A.4. Summary of the average COF loading as well as the associated uncertainty and the parameters needed for the calculations.

$\bar{L}$	Average COF loading (mg/cm^2)	1,27
$\overline{m_{COF}}$	Average COF weight (mg)	1,43
Δm_{COF}	Uncertainty associated with the weight measurement, using the laboratory scale (mg)	0,1
ΔD	Uncertainty associated with the diameter measurement, using the electrode cutter (cm)	0,001
ΔL	Uncertainty associated with the loading, calculated with Equation A.3 (mg/cm^2)	0,19

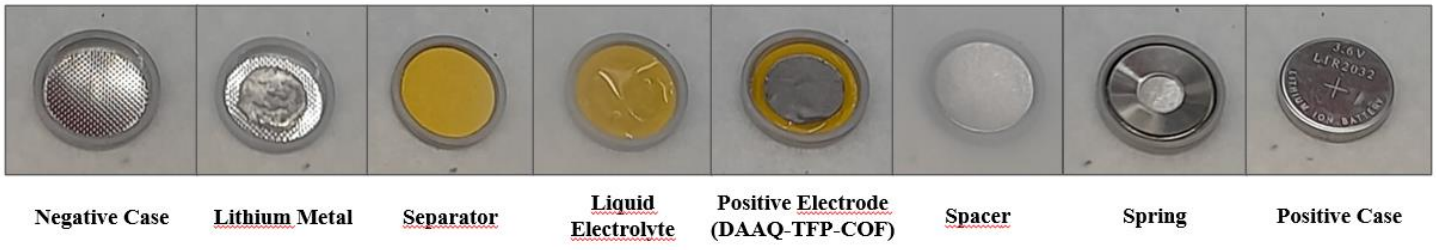

Figure A.8: Representation of the coi-cell assembly process, using pictures taken while working inside the glove box.

A.6. Summary of coin-cell results

Table A.5: Summary of the value obtained for the parameters needed for the calculation of the lithium-ion diffusion coefficient (D), for each cell.

Cell	I (mA)	T	t (s)	q (A.s)	Nº electrons	Electrons (mol)	Li^+ (mol)	C (mol/cm³)
A	0,03	2h 17 min 26 s	8246	$2{,}47 \times 10^{-1}$	$1{,}55 \times 10^{+18}$	$2{,}57 \times 10^{-06}$	$2{,}57 \times 10^{-06}$	$2{,}27 \times 10^{-04}$
B	0,03	3h 5 min 56 s	7556	$2{,}27 \times 10^{-1}$	$1{,}42 \times 10^{+18}$	$2{,}35 \times 10^{-06}$	$2{,}35 \times 10^{-06}$	$2{,}08 \times 10^{-04}$
C	0,03	13 min 24 s	804	24	$1{,}51 \times 10^{+17}$	$2{,}50 \times 10^{-07}$	$2{,}50 \times 10^{-07}$	$2{,}21 \times 10^{-05}$
D	0,03	58 min 25 s	3505	105	$6{,}57 \times 10^{+17}$	$1{,}09 \times 10^{-06}$	$1{,}09 \times 10^{-06}$	$9{,}65\times 10^{-05}$
E	0,03	2h 42 min 50 s	9770	293	$1{,}83 \times 10^{+18}$	$3{,}04 \times 10^{-06}$	$3{,}04 \times 10^{-06}$	$2{,}69 \times 10^{-04}$
F	0,03	2h 03 min 23 s	7403	222	$1{,}39 \times 10^{+18}$	$2{,}30 \times 10^{-06}$	$2{,}30 \times 10^{-06}$	$2{,}04 \times 10^{-04}$

Table A.6: Summary comparison of the important parameters obtained for each cell.

Cell	COF Weight (mg)	COF loading (mg/cm²)	OCV (V)	R_{ct} (Ohm)	CPE (F)	R_s (Ohm)	σ (-)	D (cm²/s)
A	2,01	1,78	2,570	416,4	$6{,}90 \times 10^{-06}$	4,624	887,72	$1{,}71 \times 10^{-13}$
B	2,25	1,99	2,515	120,0	$0{,}66 \times 10^{-06}$	4,503	11,093	$1{,}30 \times 10^{-09}$
C	1,27	1,12	1,101 - 2,355	345,9	$1{,}06 \times 10^{-06}$	3,283	156,38	$5{,}80 \times 10^{-10}$
D	0,77	0,68	1,942 - 2,385	622,8	$3{,}99 \times 10^{-06}$	4,100	237,47	$1{,}32 \times 10^{-11}$
E	1,03	0,91	3,007 - 3,604	649,7	$2{,}48 \times 10^{-06}$	2,704	42,978	$5{,}20 \times 10^{-11}$
F	1,25	1,11	2,112 - 2,770	162,2	$2{,}53 \times 10^{-06}$	2,707	22,570	$3{,}28 \times 10^{-10}$

Table A.7: Maximum discharge and charge specific capacities for the first and second cycles of the cells charged just in constant current (A and B).

Cell	Max DChg Capacity 1st cycle (mAh/g)	Max DChg Capacity 2nd cycle (mAh/g)	Max Chg Capacity 1st cycle (mAh/g)	Max Chg Capacity 2nd cycle (mAh/g)
A	34,17	27,43	108,98	33,47
B	41,29	35,06	120,87	43,57

Table A.8: Maximum discharge and charge specific capacities for all the cycles for the cells charged in constant current and constant voltage (C to F).

Cell	Maximum Specific DChg Capacity (mAh/g)	Maximum Specific Chg Capacity (mAh/g)
C	30,348	47,089
D	73,111	99,321
E	83,746	114,072
F	83,155	113,590

A.7. Data for each cell

- **Cell A**

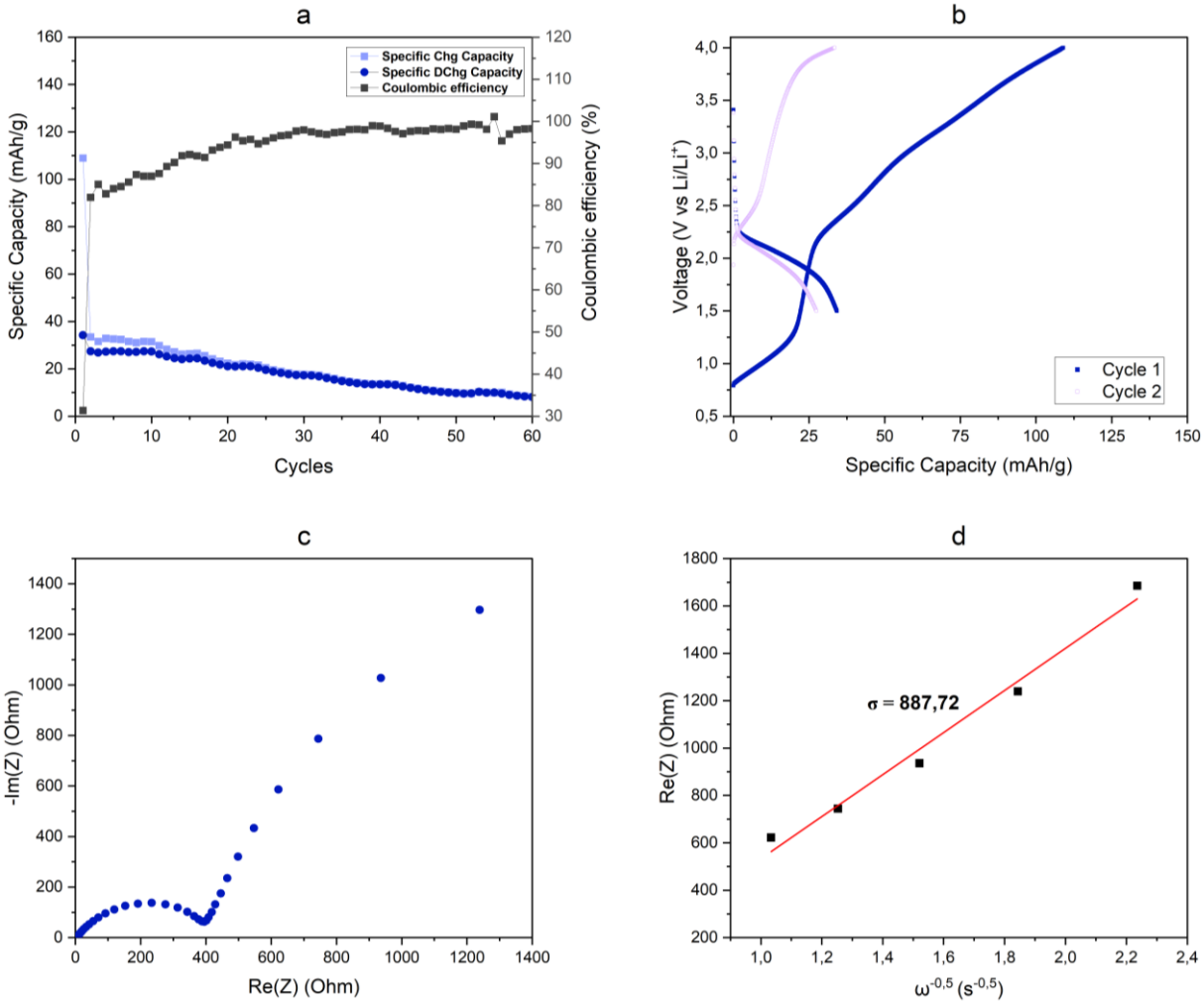

Figure A.9:Electrochemical performance of cell A (a) Cycling performance until cycle number 60 and the respective Coulombic Efficiency. (b) Charge-Discharge curves for cycles 1 and 2. (c) Nyquist plot obtained through PEIS. (d) Plot to determine the Warburg coefficient

- **Cell B**

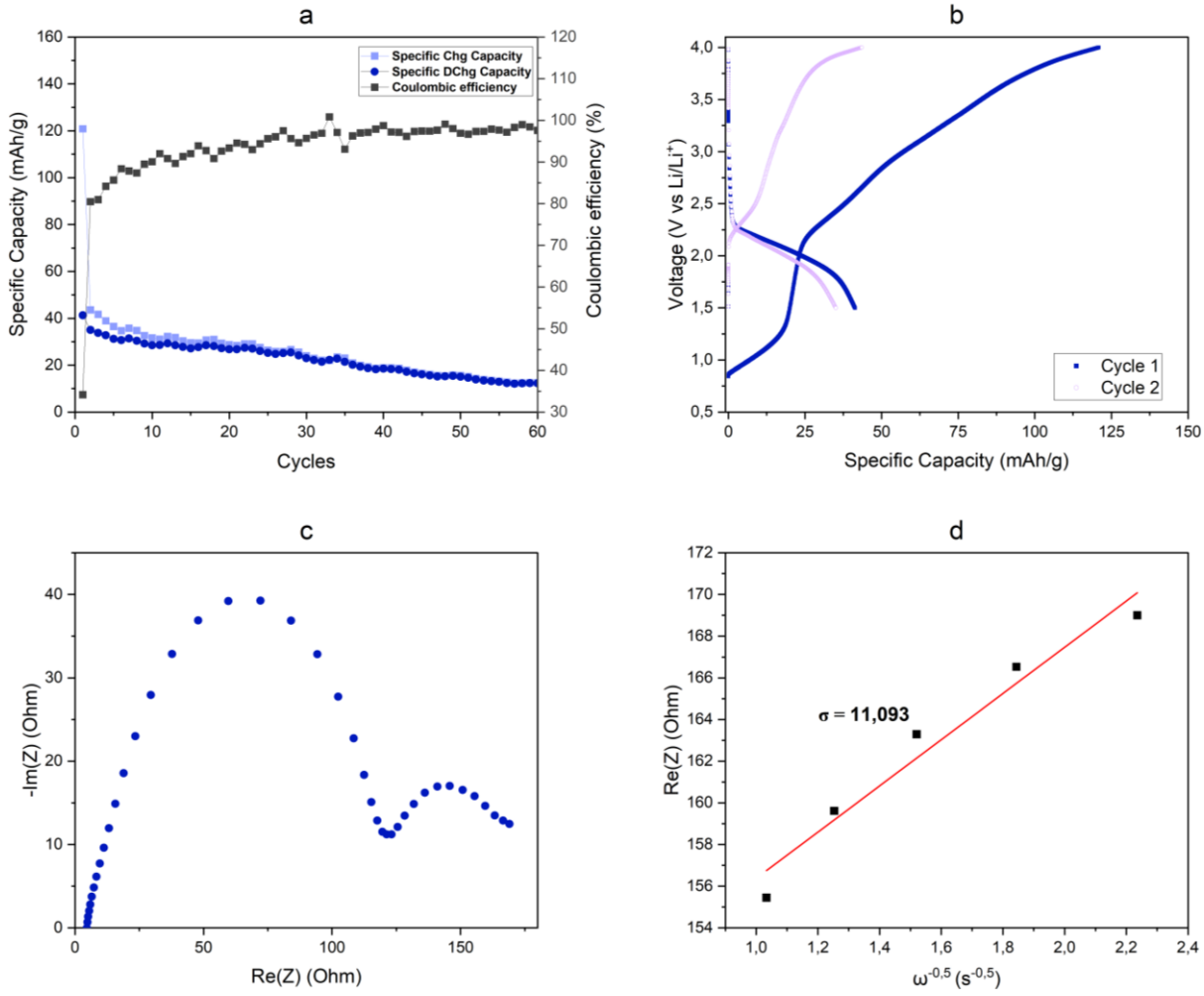

Figure A.10: Electrochemical performance of cell B (a) Cycling performance until cycle number 60 and the respective Coulombic Efficiency (b) Charge-Discharge curves for cycles 1 and 2 (c) Nyquist plot obtained through PEIS (d) Plot to obtain the Warburg coefficient

- **Cell C**

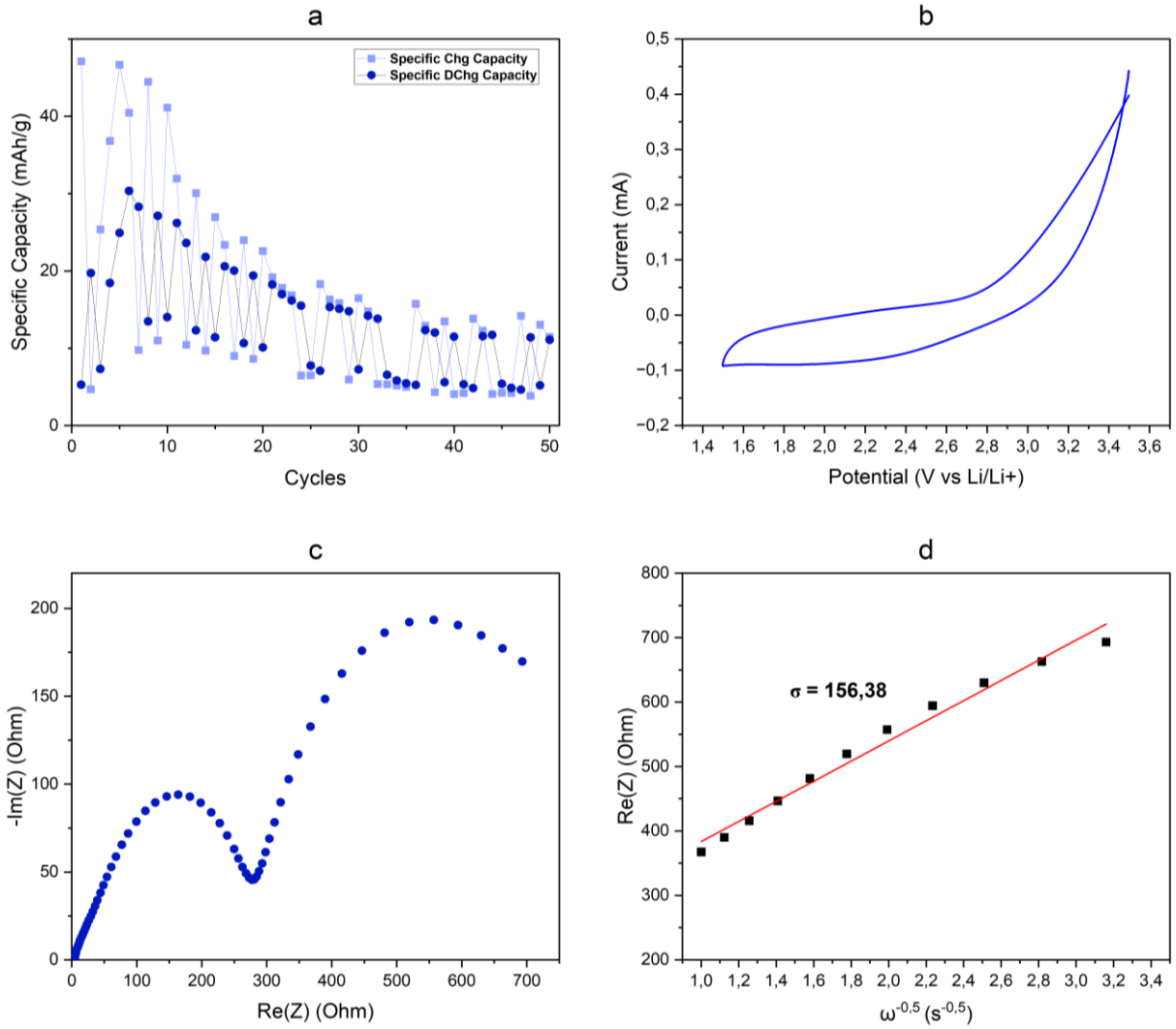

Figure A.11: Electrochemical performance of cell C (a) Cycling performance until cycle number 60 and the respective Coulombic Efficiency. (b) Cyclic voltammogram at 5 mV/s (c) Nyquist plot obtained through PEIS. (d) Plot to determine the Warburg coefficient

- **Cell D**

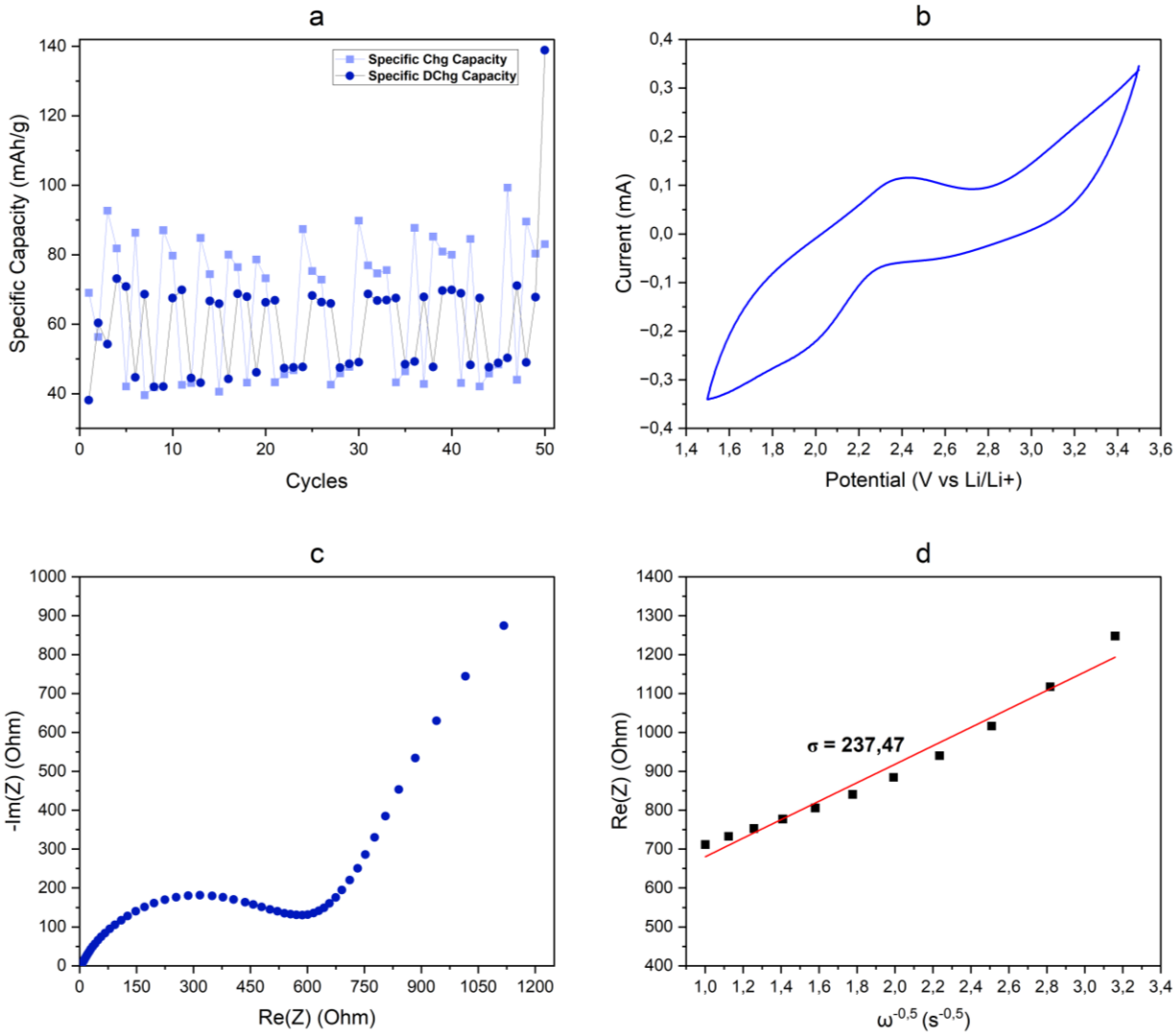

Figure A.12: Electrochemical performance of cell D (a) Cycling performance until cycle number 60 and the respective Coulombic Efficiency. (b) Cyclic voltammogram at 5 mV/s (c) Nyquist plot obtained through PEIS. (d) Plot to determine the Warburg coefficient

- **Cell E**

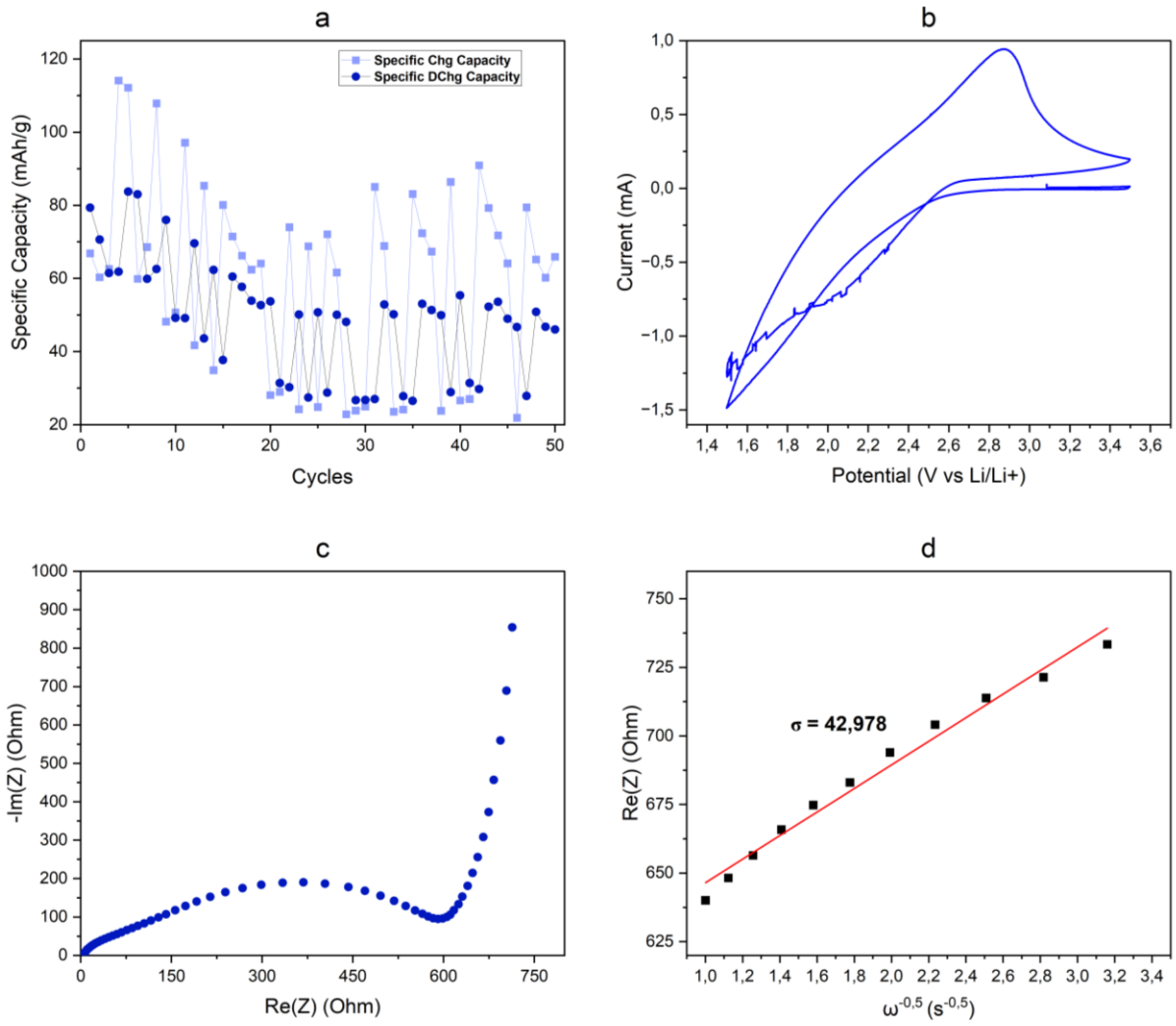

Figure A.13: Electrochemical performance of cell E (a) Cycling performance until cycle number 60 and the respective Coulombic Efficiency. (b) Cyclic voltammogram at 5 mV/s (c) Nyquist plot obtained through PEIS. (d) Plot to determine the Warburg coefficient

- **Cell F**

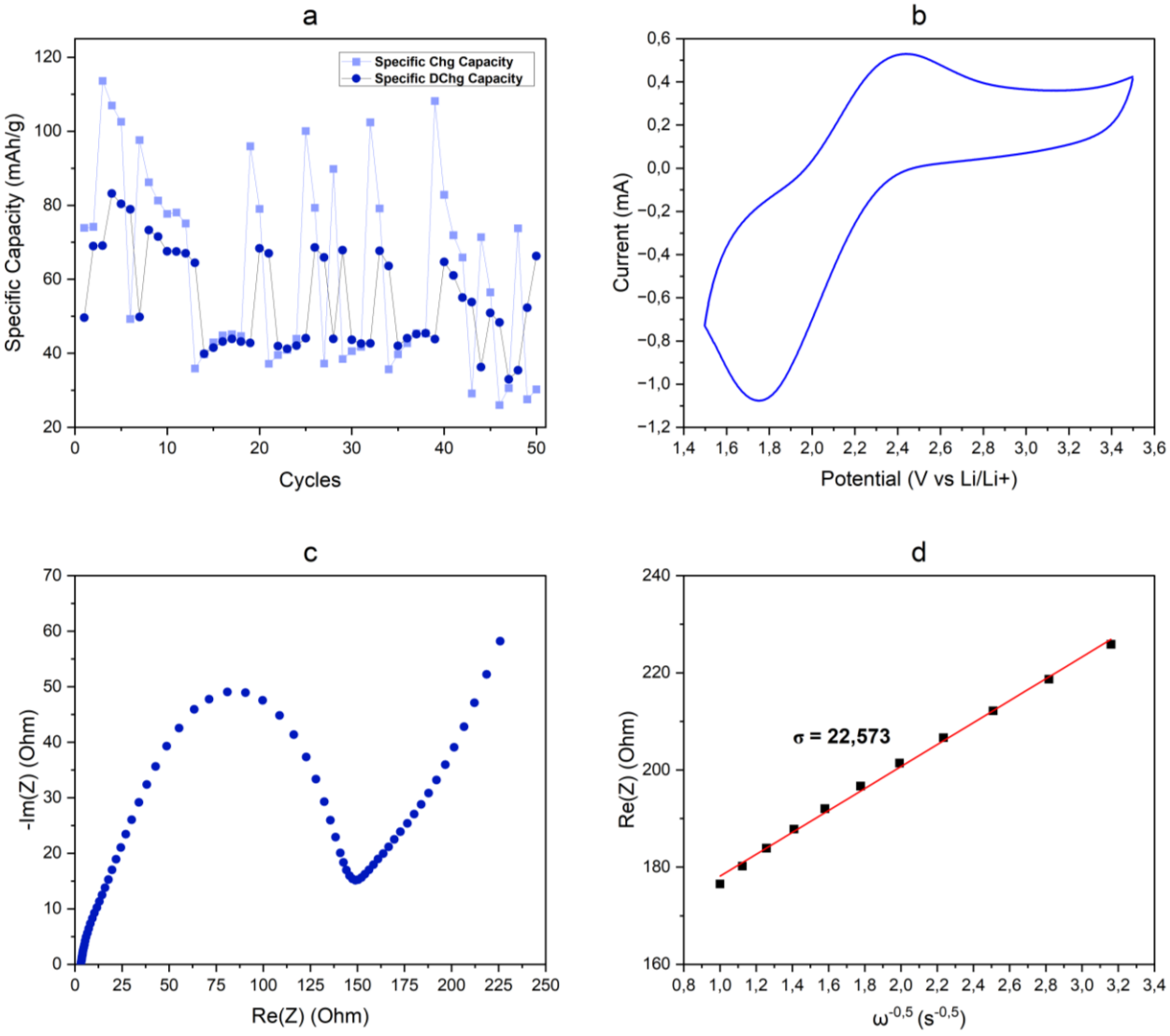

Figure A.14: Electrochemical performance of cell F (a) Cycling performance until cycle number 60 and the respective Coulombic Efficiency. (b) Cyclic voltammogram at 5 mV/s (c) Nyquist plot obtained through PEIS. (d) Plot to determine the Warburg coefficient

A.8. Additional images

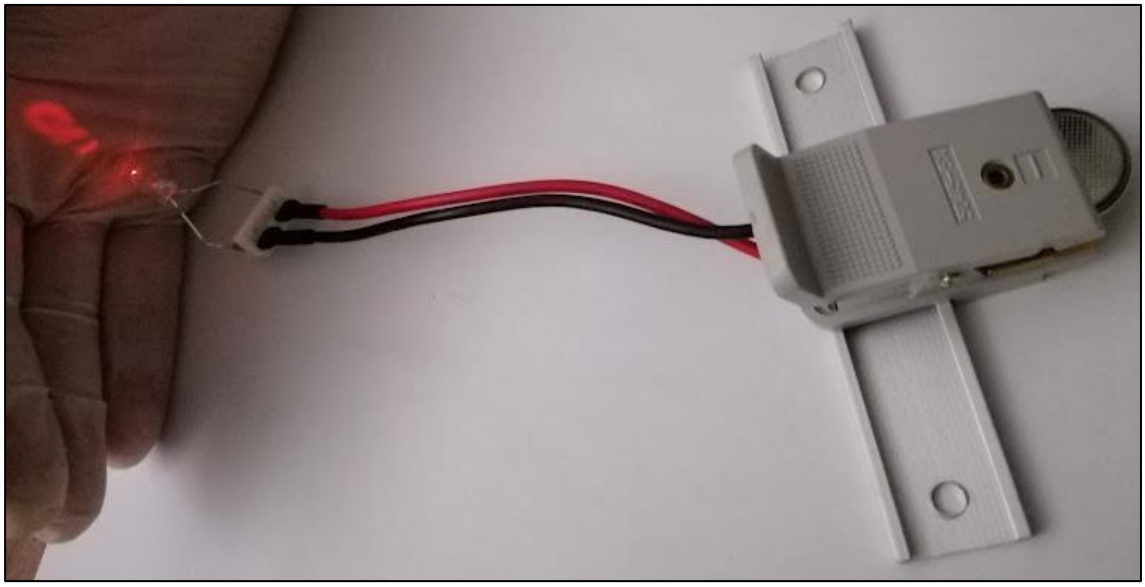

Figure A.15. Half-cell, coin-cell, with DAAQ-TFP-COF as positive electrode, lightening a red LED.

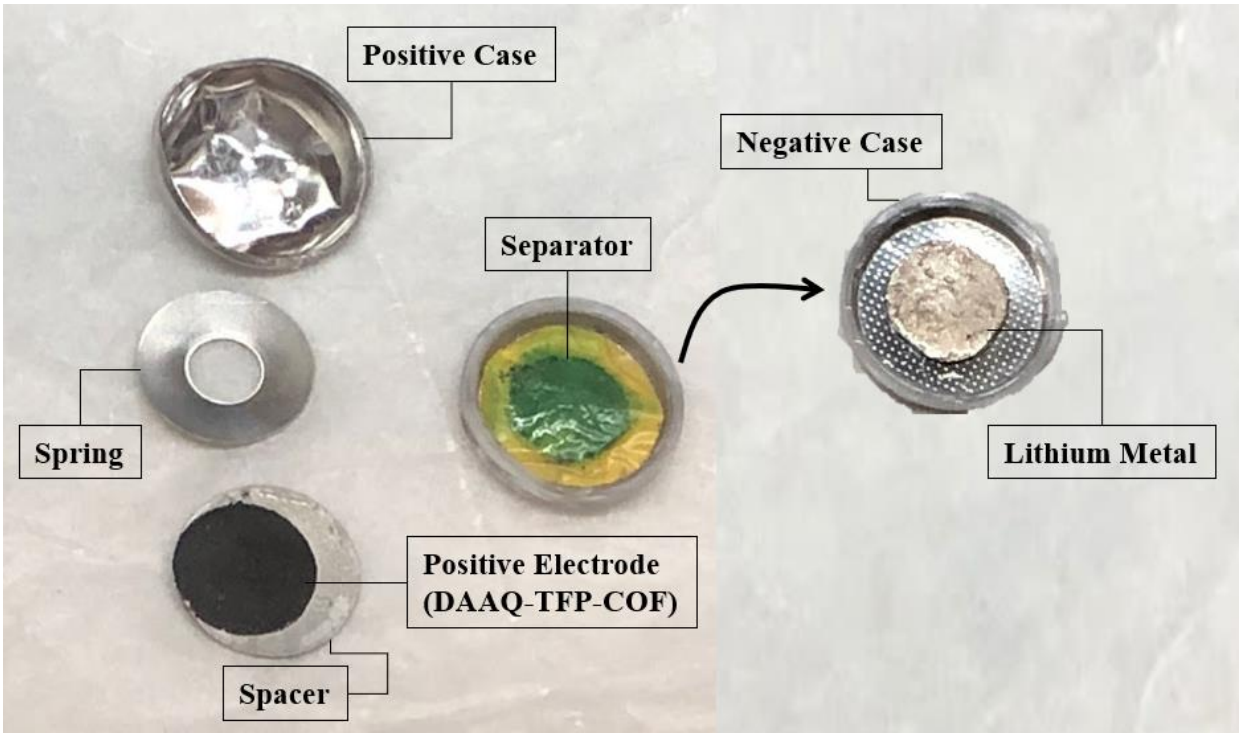

Figure A.16. Parts of the coin-cell after opening and disassembly